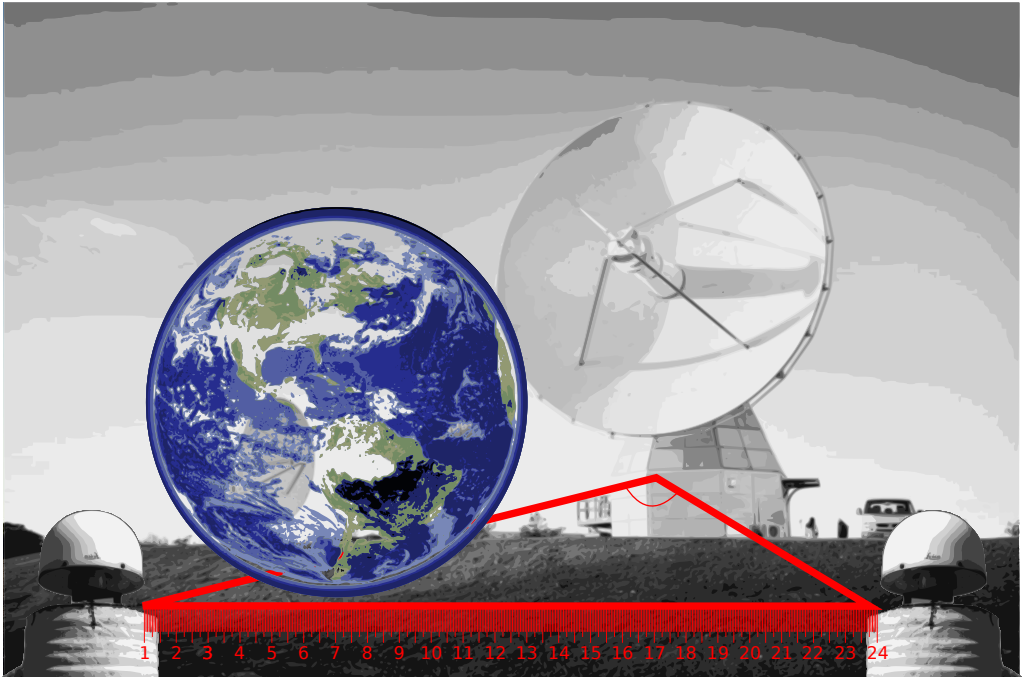




CHALMERS



Exploring Strategies for the Combination of Multiple Space-geodetic Techniques

PERIKLIS-KONSTANTINOS DIAMANTIDIS

THESIS FOR THE DEGREE OF LICENTIATE OF ENGINEERING

Exploring Strategies for the Combination of Multiple
Space-geodetic Techniques

PERIKLIS-KONSTANTINOS DIAMANTIDIS

Department of Space, Earth and Environment
Onsala Space Observatory
CHALMERS UNIVERSITY OF TECHNOLOGY
Gothenburg, Sweden 2020

Exploring Strategies for the Combination of Multiple Space-geodetic Techniques
PERIKLIS-KONSTANTINOS DIAMANTIDIS

© PERIKLIS-KONSTANTINOS DIAMANTIDIS, 2020

Department of Space, Earth and Environment
Onsala Space Observatory
Chalmers University of Technology
SE-412 96 Gothenburg
Sweden
Telephone: +46 (0)31-772 1000

Chalmers Reproservice
Gothenburg, Sweden 2020

Exploring Strategies for the Combination of Multiple Space-geodetic Techniques
PERIKLIS-KONSTANTINOS DIAMANTIDIS
Department of Space, Earth and Environment
Chalmers University of Technology

Abstract

Space-geodetic techniques are based on signal acquisition from extraterrestrial radio sources that can be used to infer geodetic positioning and define Earth-fixed and inertial reference systems. These techniques, which include Very Long Baseline Interferometry (VLBI) and Global Navigation Satellite Systems (GNSS) among others, exhibit different strengths and weaknesses in recovering parameters of interest. VLBI, for example, has access to all parameters linking Earth-fixed and inertial reference systems, so-called Earth Orientation Parameters (EOP), while GNSS is superior at determining in one of the EOP, Polar Motion (PM), due to the ubiquity and global distribution of the GNSS network of permanent receivers. The combination of different space-geodetic techniques shows promise in suppressing technique-specific biases and determining parameters with greater precision. This thesis presents the principles of VLBI and GNSS, and then explores the different combination strategies that can be used in the aim of generating of high-quality space-geodetic products.

Keywords: GNSS, VLBI, Combination on the Observation Level, Space Geodesy, Local Ties, Reference Systems, EOP

Acknowledgements

I would like to thank my supervisor Dr. Rüdiger Haas for the support he has given me during my tenure as doctorate candidate in Chalmers. I would also like to thank my mentor Dr. Thomas Hobiger for his immeasurable help in research matters and for the development of specified modules in the `c5++` space geodetic software. My colleagues in the department always create a convivial atmosphere and a happy working environment. A special mention goes towards Dr. Grzegorz Kłopotek, my office mate, for an excellent cooperation during the past 2.5 years. Finally, I would like to thank my family for their ever-lasting support and my friends for putting up with me.

Publications

This thesis is based on the work contained in the following papers:

- I P.-K. Diamantidis et al. (2020). VLBI and GPS inter- and intra-technique combinations on the observation level for evaluation of TRF and EOP. *Earth, Planets and Space*. in review

Contents

Abstract	i
Acknowledgements	iii
Publications	v
Contents	vii
1 Introduction	1
1.1 Outline of the thesis	2
2 Space Geodesy	3
2.1 Reference Systems	3
2.2 Time Systems	5
2.2.1 Sidereal and Universal Time	5
2.2.2 Atomic Time	6
2.3 Atmospheric Refraction	6
2.3.1 Tropospheric Delay	6
2.3.2 Ionospheric Delay	9
2.4 Displacements	10
3 Global Navigation Satellite Systems	11
3.1 Basic GNSS Observables	12
3.2 Receiver Clock Treatment	15
3.3 GNSS in Space Geodesy	15
4 Very Long Baseline Interferometry	19
4.1 Basic VLBI Observables	20
4.1.1 Correlation	20
4.1.2 Scheduling	23
4.2 VLBI Delay Model	23
4.3 Data Analysis	25
4.3.1 Datum Constraints	25
4.3.2 Parameter Constraints	26
4.4 VLBI in Space Geodesy	26
5 Combination of Space-geodetic Techniques	29
5.1 Combination Strategies	30
5.1.1 Combination on the Results Level	30
5.1.2 Combination on the Normal Equation Level	30
5.1.3 Combination on the Observation Level	31
5.2 Local Ties	31
5.3 A Novel Approach to Combination	32
6 Summary and outlook	37
Bibliography	38

Chapter 1

Introduction

There is something inherently incompatible between the human condition and Metrology. People are subconsciously biased towards conformism, which can be described as determinism on a very short time scale. This is evident in their susceptibility to easy answers and propensity to follow opportunistic change. Metrology, on the other hand, follows the exact inverse route. It initially establishes an uncertainty band and it actively works to diminish it. The stochasticity that precludes definiteness is followed by an evolving suppression of biases and confidence intervals, and the eventual establishment of inertial references unmoved by opportunistic or spurious signals. This process lies at the core of every metrological science, and when applied to the study of the size, shape, orientation and gravitational field of the Earth, in Space Geodesy.

The necessity for precise definitions of terrestrial and celestial reference frames and the determination of parameters that describe the Earth's orientation in inertial space, so-called Earth Orientation Parameters (EOP) are central to this field. In order to achieve this goal, different space-geodetic techniques were developed, i.e., techniques that rely on signals from extraterrestrial sources to infer frame definitions and EOP. These techniques include Very Long Baseline Interferometry (VLBI), Global Navigation Satellite Systems (GNSS), Satellite Laser Ranging (SLR), Lunar Laser Ranging (LLR) and Doppler Orbitography and Radiopositioning Integrated by Satellite (DORIS). When used independently, they suffer from technique-specific systematic errors and, apart from VLBI, are limited in the EOP that they are sensitive to. The active suppression of said errors can be partially achieved by improved modelling and equipment but in a metrological sense it can only ultimately come from the diversification of information that infer parameters of interest. In other words, the meaningful combination of said techniques holds the promise of ever more precise determinations.

In this context, the International Earth Rotation and Reference Systems Service (IERS) has established and operated working groups towards examining different methods of rigorous combination of space-geodetic techniques (Gambis et al., 2012). In parallel the concept of fundamental stations, i.e., sites that are able to record observations from multiple space-geodetic techniques, has risen in prominence given

the potential that simultaneity and temporal correlation gives between different observables.

1.1 Outline of the thesis

This thesis delves deeper into the topic of different methods to achieve combination of multiple space-geodetic techniques. In particular, Chapter 2 gives an introduction into the common framework which is present in all space-geodetic techniques, namely spatio-temporal reference frames and common parameters of interest that are estimated during data analysis. Chapters 3 and 4 present basic concepts of GNSS and VLBI, respectively, that need to be taken into account during the estimation and/or combination process and their contributions to space-geodetic products. Different combination schemes analysed in Chapter 5 along with the Paper I contribution of this thesis. Finally, Chapter 6 provides a summary and outlook.

Chapter 2

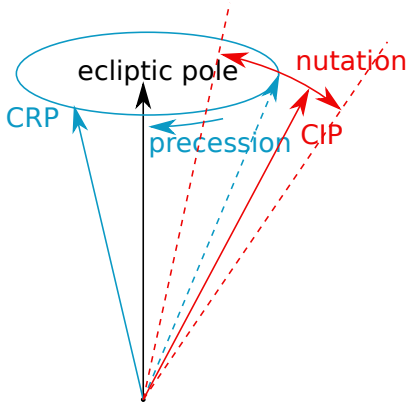
Space Geodesy

Space-geodetic techniques share a common mode of operation. Earth-based stations collect and time-tag signals, coming either from an extra-galactic source, an artificial satellite or the Moon. The stations, positioned on the Earth's crust, are affected by a plethora of geodynamical phenomena that perturb their position. The signals experience some form of refraction when propagating through the atmosphere which distorts their path. The collected data are processed with the aim of aiding in the establishment of stable reference frames. A description of the reference systems and frames as well as error sources common to most techniques that occur during this signal propagation and acquisition process follows.

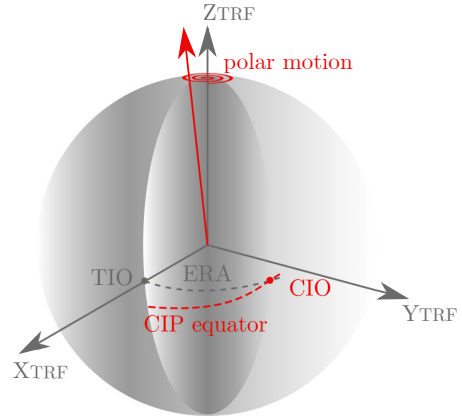
2.1 Reference Systems

The definition, realisation and maintenance of reliable reference systems is essential for space-geodetic applications that rely on the utmost precision, in order to quantify, separate and study different geodynamical phenomena and parameters of interest. While reference systems are the theoretical framework consisting of the goals, conventions and formalisations used, the actual realisation comes in the form of reference frames. These frames consist of a robust catalogue of coordinates of well-defined points, which enable users to gain access to high quality geodetic products.

To fulfill this goal, both Earth-fixed and inertial reference systems and frames have been developed. One of the well-established Earth-fixed or terrestrial reference systems is the so-called International Terrestrial Reference System (ITRS). The ITRS is realised as the International Terrestrial Reference Frame (ITRF) through the determination of zeroth and first time-derivatives of its origin, orientation and scale. The ITRF is maintained and routinely updated by the IERS, with the latest version designated as the ITRF2014 (Altamimi et al., 2016). The International Celestial Reference System (ICRS) is the counterpart of ITRS in the inertial space. Its origin is at the barycenter of the solar system although an equivalent system with a different origin definition, that of the geocenter, is also used, the Geocentric Celestial Reference System (GCRS). The realisation of the ICRS is predominantly



(a) The nutation/precession movement along with the Celestial Intermediate Pole (CIP) to Celestial Reference Pole (CRP) transformation. Notice that the effect of nutation is exaggerated for illustration purposes.



(b) The polar motion and the definition of the Earth Rotation Angle (ERA). The latter is the angle that corresponds to the arc between the Celestial Intermediate Origin (CIO) and Terrestrial Intermediate Origin (TIO).

Figure 2.1: Representations of the nutation/precession in (a) and polar motion in (b).

used by the International Astronomical Union (IAU) and maintained by the IERS in the form of the International Celestial Reference Frame (ICRF) with its latest version, the ICRF3 (Charlot et al., 2020).

The Earth's motion can be described as an axis-angle rotation where the axis of rotation itself is changing orientation. This change is the superimposition of rotational movements with different periodicities, a key feature that allows for their separation and study (Petit and Luzum, 2010). In particular, the orientation of the rotation axis is changing with respect to the Earth's crust, a phenomenon which is called polar motion (PM). Earth's rotation axis also shows an obliquity, i.e., an axial tilt, with respect to its orbital plane around the sun, i.e., the ecliptic plane. This tilt is not constant but shows a small variation over time, described by nutation. The rotation axis, retrieved by the mean obliquity, is in turn rotating with respect to the ecliptic pole, a phenomenon called precession. Fig. 2.1a shows the nutation/precession effect separately, i.e., the trace of the combined movement of the CIP is not visible.

The rotation axis is always perpendicular to the equatorial plane of a reference system. The origin of the longitude in the equatorial plane of the Earth-fixed system known as the Terrestrial Intermediate Origin (TIO) is rotating with respect to the origin of the right ascension of the Celestial Intermediate Pole (CIP) equator, so-called Celestial Intermediate Origin (CIO). The angle that is formed between them is called Earth Rotation Angle (ERA), as shown in Fig.2.1b. Space-geodetic techniques can be used for determining corrections on the precession/nutation

model (also called celestial pole offsets, dX , dY), the x- and y-component of the polar motion (x_p , y_p), and the *ERA*, or the equivalent concept of Universal Time (*UT1*). This completes the axis-angle description of the motion of the Earth, and the set of these five parameters constitute the EOP.

The transformation procedure between the GCRS and the ITRS is as follows (Petit and Luzum, 2010)

$$\vec{X}_{GCRS} = Q(t)R(t)W(t)\vec{X}_{ITRS}, \quad (2.1)$$

where $Q(t)$ is the composite rotation matrix for precession/nutation, $R(t)$ the rotation matrix for Earth rotation and $W(t)$ the one for polar motion. As Eq. 2.1 shows, the transformation between the two reference systems is reminiscent of the procedure normally applied to the transition between orbital planes of common origin, eccentricity and size of semi-major axis. Three elemental rotations are used around the two of the three axes attached to the orbital plane, with angles (a) u_0 or argument of the latitude, (b) i or inclination and (c) Ω or right ascension of the ascending node.

2.2 Time Systems

Space Geodesy is based on recording the time of arrival of signals, either from or to a satellite or another extraterrestrial source and their subsequent correlation in order to extract a time-delay. As important as it is to define a precise reference frame in the confines of the three-dimensional space, the same is equally true to time. The concept of hour angle finds widespread use in this context. Hour angle is the angle between the local meridian and the path pointing to the vernal equinox, i.e., the CIO.

2.2.1 Sidereal and Universal Time

The transformation of the hour angle in time units, provides the so-called sidereal time. This time definition suffers from both irregularities in Earth's rotation but also from the effects that precession and nutation have on the CIP equator. The concept of a "true" vernal equinox, which materialises after removing the bias induced by the precession effect gives what is known as the Local Apparent Sidereal Time (LAST). Correcting for both precession/nutation gives the "mean" vernal equinox and the so-called Local Mean Sidereal Time (LMST). If instead of the local meridian, the Greenwich meridian is used, LMST and LAST are converted to GMST and GAST where "G" stands for Greenwich. Tracing a "mean" Sun (since the true movement of the Sun is not uniform) instead of the CIO can be used, which enables the Universal Time (*UT*) to be retrieved. If the effect of the polar motion is removed the *UT* transforms to *UT1*. The *UT1* parameter is linked to *ERA* through a linear relationship (Capitaine, 2008)

$$ERA(T_u) = 2\pi(0.7790572732640 + 1.00273781191135448T_u), \quad (2.2)$$

where $T_u = (\text{Julian } UT1 \text{ date} - 2451545.0)$.

2.2.2 Atomic Time

The state-of-the-art time scale which is used today is the Atomic Time (*TAI* - Temps Atomique International) which is maintained by the IERS and the Bureau International des Poids et Mesures (BIPM). The weighted average of a number of free-running atomic clocks is computed in the form of the Free Atomic Scale (EAL - Échelle Atomique Libre). This is then steered to maintain agreement with the SI definition of a second (Petit et al., 2015). Since *UT1* is affected by the gradual deceleration of the angular velocity of the Earth's rotation, there are ever growing discrepancies with respect to *TAI*. To keep track of these, the Coordinated Universal Time (*UTC*) has been introduced, which is a discretized approximation on the level of seconds of *UT1* and has its basis on *TAI*, i.e.,

$$UTC = TAI + ls, \quad (2.3)$$

where *ls* are the leap seconds added, so that *UT1* – *UTC* is maintained in the sub-second level. When estimating EOP, instead of *UT1*, the *UT1* – *UTC* value is also used, along with the excess revolution time, or Length of Day (*LOD*).

2.3 Atmospheric Refraction

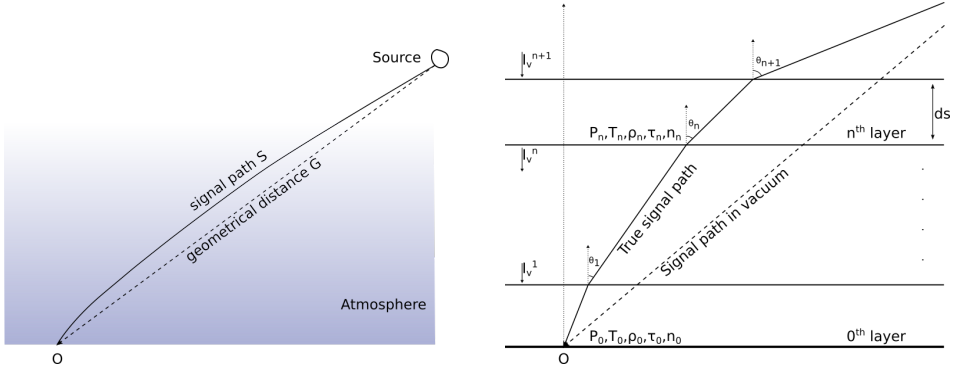
The distortion of the signal paths as they propagate through the atmosphere is a common error source in all microwave-based space-geodetic techniques. The physical phenomena that cause it are (a) the induced and permanent dipole moments of neutral atmospheric gases and water vapor respectively, resulting in what is commonly referred to as tropospheric delay, and (b) the dispersion due to the free electrons in the ionosphere, leading to the so-called ionospheric delay.

2.3.1 Tropospheric Delay

Any signal travelling through the neutral atmosphere experiences refraction which leads to an alteration of both of its path as shown in Fig. 2.2a and phase velocity. The layered atmosphere approximation can lead to determination of the signal path delay. The magnitude of the phase velocity at layer *n*, $v_{ph,n}$, can be retrieved from the refractive index n_n since by definition $n_n = \frac{c}{v_{ph,n}}$. The change of the signal path when it enters layer *n* can be determined by the ratio of the refractive indices through Snell's law, $\frac{\sin\theta_{n+1}}{\sin\theta_n} = \frac{n_n}{n_{n+1}}$, where θ is the angle measured from the normal of the boundary. Details are present in Fig. 2.2b. The time delay t_d of the arrival of the signal is $t_d = \int_S \frac{1}{v_{ph}(s)} ds - \int_G \frac{1}{c} dg$, which can be converted to path length as

$$\Delta L^T = \int_S (n(s) - 1) ds + S - G. \quad (2.4)$$

As we see in Eq. 2.4, the delay term ΔL^T takes into account the geometry of the two paths *S* and *G*, which constitutes the “geometric delay”, and the divergence of the phase velocity in the atmosphere from the value it has in vacuum. Notice that



(a) True, S , and geometrical, G , signal path.

(b) Ray tracing through a horizontally stratified atmosphere.

Figure 2.2: The “bending” of the signal path due to the refraction in the atmosphere. Instead of following the geometrical path, G , the true signal path, S , is presented. Note that the effect is exaggerated for the purposes of illustration.

$n(s) - 1$ in Eq. 2.4 can be alternatively written as $n(s) - n_{vacuum}$ as the refractive index in vacuum is equal to 1. It is also worth noting that through Snell’s law, for a horizontally stratified atmosphere, a signal at zenith, i.e., with angle $\theta = 0$ will not experience refraction and thus paths S and G will be identical. In this case the so-called path delay at zenith, $\Delta L^{T,z}$, will be solely dependent on the change in phase velocity.

The path delay contains the accumulated effect of all atmospheric gases, the water vapor and the liquid water and can be split up into “dry” and “wet” parts, $\Delta L^T = \Delta L_{dry}^T + \Delta L_{wet}^T$ (Davis et al., 1985). The contribution of most of the “dry” atmospheric components can be concentrated in the first term and can be shown to be modelled well using measured total pressure at ground level. The wet term ΔL_{wet}^T cannot be easily inferred due to poor correlation between water vapor density on the ground and at different altitudes. It becomes, therefore, an error source that must be estimated and removed from space-geodetic observables. The most prominent way of accomplishing this is by approximating it as a linear function of the “wet” delay at zenith, $\Delta L_{wet}^T = m f_w \Delta L_{wet}^{T,z}$ where the term $m f_w$ is an elevation-dependent mapping function. The coefficients that may complement a mapping function can be a result of empirical data or global grid models (Boehm et al., 2006; Landskron and Böhm, 2018).

Another way of looking at tropospheric delay is by approximating the troposphere as an inverse cone with its tip at the receiver point, a radius of 65 km and a height of the tropopause between 9 km and 17 km (Walpersdorf et al., 2001). Mapping functions inflate the estimated delay at zenith with an elevation-dependent value. They are, therefore, insensitive to azimuthal variations. Signals that arrive in concentric rings per elevation angle are approximated as experiencing the same delay. The effect is visible in Fig. 2.3. A more sophisticated approach attempts to

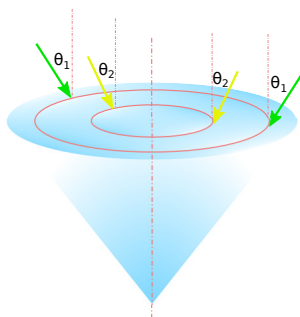


Figure 2.3: For a homogeneous atmosphere all signals with the same angle of incidence experience the same delay irrespective of azimuthal direction. The difference in delay is thus only visible for groups of signals of different angles like, e.g., the green ones (angle θ_1) in contrast to the yellow ones (angle θ_2).

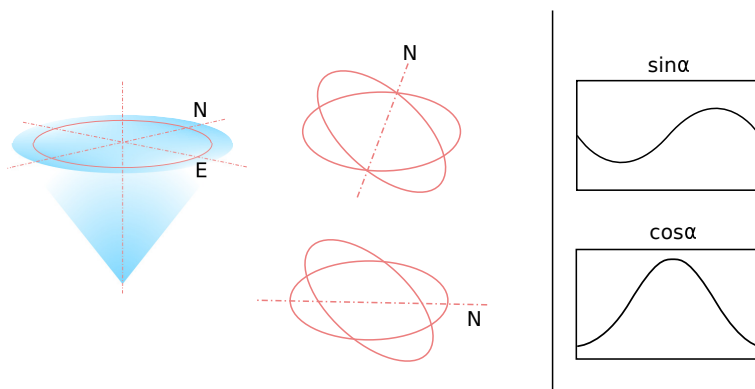


Figure 2.4: For an inhomogeneous atmosphere there is an azimuthal variation of the troposphere delay, shown on the right, as a response to a rotation of the base plane of the cone around the north (top) and the east (bottom) axis.

tilt the base of the inverted cone, denoting the presence of a gradient. As Fig. 2.4 shows, rotation around the north axis gives a variation of a sine pattern along the trace of the circle with the maximum/minimum occurring in the east/west direction, G_E , while a rotation around the east axis gives a cosine pattern with maximum/minimum in the north/south direction, G_N . One can thus augment the wet tropospheric delay by

$$\Delta L_{wet}^T = mf_w \Delta L_{wet}^{T,z} + mf_g (G_N \cos \alpha + G_E \sin \alpha), \quad (2.5)$$

where mf_g a gradient mapping function and α the azimuth angle.

2.3.2 Ionospheric Delay

The ionosphere is, as opposed to the troposphere, a dispersive medium. This means (a) that the phase velocity is frequency-dependent and (b) that the group and phase velocities are different. The latter can be inspected via the relation between the angular frequency ω and the wave number k , which is described as

$$\omega^2 = c^2 k^2 + \omega_p^2, \quad (2.6)$$

where $\omega_p = 2\pi f_p$, $f_p = 8.98\sqrt{N_e}$ and N_e the electron density. Since phase velocity is $v_{ph} = \frac{\omega}{k}$ and group velocity is $v_{gr} = \frac{d\omega}{dk}$, they can only be equal if ω and k are directly proportional, something that Eq. 2.6 clearly violates. The magnitude and relation between group and phase ionospheric delays can be established (Petit and Luzum, 2010). In particular, they have inverse signs and equal magnitudes which for the case of the phase delay is

$$\Delta L_p^I(f) = -\frac{s_1}{f^2} - \frac{s_2}{f^2} - \frac{s_3}{f^2}, \quad (2.7)$$

where s_1 , s_2 and s_3 are first second and third order terms. These are equal to (Petit and Luzum, 2010)

$$\begin{aligned} s_1 &= 40.309 \int_L N_e dl, \\ s_2 &= 1.1284 \cdot 10^{12} \int_L N_e B \cos \theta dl, \\ s_3 &= 812.42 \int_L N_e^2 dl + 1.5793 \cdot 10^{22} \int_L B^2 (1 + \cos^2 \theta) dl, \end{aligned} \quad (2.8)$$

where B is the geomagnetic field modulus, θ the angle between the signal and the geomagnetic field. Integrating the electron density over the total path gives the Slant Total Electron Content

$$STEC = \int_L N_e dl, \quad (2.9)$$

which incorporated in the first-order term s_1 of Eq. 2.8 gives the phase ionospheric delay as

$$\Delta L_p^I(f) \approx -\frac{40.309}{f^2} STEC. \quad (2.10)$$

This is an approximation that neglects the higher-order terms which may need to be incorporated, depending on the application (Petit and Luzum, 2010). It is important to note that the total electron content (TEC) exhibits diurnal variations as the Sun affects the ionisation of the upper atmosphere, as well as the aforementioned frequency dependence of the ΔL_p^I (and also ΔL_g^I) as shown in Eq. 2.10. The main ways to mitigate ionospheric delay are (a) to observe at multiple frequencies and combine measurements so that the effect of the ionosphere is removed or (b) through the use of empirical models or space-geodetic observables to produce world grids of TEC the so-called vertical TEC (VTEC) maps. These are distributed in specialised data formats, an example of them being the Ionosphere map Exchange format (IONEX) (Hernández-Pajares et al., 2009). The first-order approximation removes most of the ionospheric effect but VTEC products also allow for the mitigation of the higher-order terms.

2.4 Displacements

Geodynamical phenomena that are triggered by either the gravitational attraction between Earth and other celestial bodies, or a direct result of the endogenic processes of the Earth itself, result in a variability of station coordinates over time. The motion can be decomposed in tidal and non-tidal effects. First-order tidal effects due to luni-solar attraction, also known as solid Earth tides (Agnew, 2015), and second-order effects like the elastic response of the Earth's crust to (a) ocean tides (ocean loading) (Scherneck and Webb, 1999), (b) the differential in atmospheric pressure with respect to time (atmospheric loading) (Boy et al., 1998), (c) the shift in Earth's axis of rotation (pole tide) (Miller and Wunsch, 1973). The combined effect can reach up to a level of tens of centimeters. Non-tidal components of the above are also present (Williams and Penna, 2011), as well as local variations maybe present like interseismic (Biggs et al., 2007) or postseismic deformations (Hearn et al., 2009) of the Earth's crust, which can significantly affect geodetic measurements (MacMillan et al., 2012).

Chapter 3

Global Navigation Satellite Systems

The principles of Global Navigation Satellite Systems (GNSS) were first demonstrated in the 1950's and early 1960's as a technique used for satellite tracking by measuring the frequency Doppler shift with respect to a ground station of known position. Equivalently in a reverse process, satellites that inhabit known orbits can be used to determine geodetic positioning of a ground station. This concept was explored by the TRANSIT system, the first such satellite system with global coverage (Kumar and Moore, 2002).

Modern GNSS, such as the Global Positioning System (GPS), rely on range measurements between their space-based segment, i.e., a satellite constellation, and the ground-based segment, i.e., receivers. The time of arrival (TOA) of a signal transmitted by a GPS satellite is determined at the receiver, allowing for a range to be estimated. Since range is a one-dimensional quantity and therefore lacks information about the direction of the transmitter, three measurements would be needed to establish the position of the receiver, in a process known as trilateration (Fig. 3.1). In reality, biases induced because of timing inconsistencies between transmitter and receiver clocks, mean that a fourth measurement needs to be added in order for the positioning of the receiver to be determined with reasonable accuracy, with more measurements contributing to the over-determination of the problem and thus increased accuracy.

While, as the name suggests, GNSS are used in the field of navigation, they have found multi-disciplinary use in, among others, satellite tracking, remote sensing and Space Geodesy (Jin et al., 2014; Prange et al., 2017; Springer et al., 2011). For the latter in particular, it is forming a part of the satellite geodesy branch. The establishing of permanently installed GNSS receivers in a dense worldwide network and the subsequent acquisition and analysis of GNSS data, has developed products that support the monitoring of Earth's rotation and polar motion and the study of geodynamical phenomena like, e.g., crustal deformation or tectonic plate movement (Brockmann et al., 2012; Noll, 2010). This activity mainly takes place through the International GNSS Service (IGS), an association of research institutes worldwide that voluntarily maintains and updates space-geodetic products (Johnston et al., 2017).

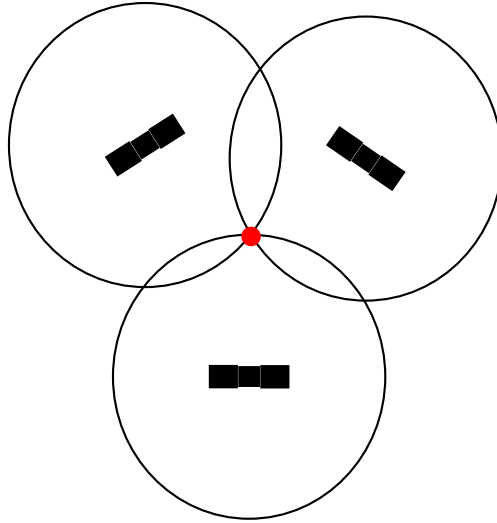


Figure 3.1: *Visualisation of the trilateration procedure for determination of a point in 2D space. The satellites (black) send out signals that are received at the receiver (red). By intersection of the circles the receiver's position is determined.*

The first fully operational GNSS was GPS, which is now complemented by several other systems that offer global coverage, namely, the Russian GLONASS, the European Galileo, and the Chinese Beidou. A multi-GNSS experiment (MGEX), has been initiated by IGS with the aim of exploring the new capabilities that the combination of different GNSS can offer (Montenbruck et al., 2017).

3.1 Basic GNSS Observables

Modern GNSS receivers determine the range between the transmitter and the receiver in two different ways.

- Firstly, by cross-correlating the incoming signal with a signal replica that the receiver produces using its own internal clock and acquiring the time of arrival (TOA), the so-called code-phase measurement.
- Secondly, by counting the total number of cycles that the carrier wave of the incoming signal has travelled, the so-called carrier-phase measurement.

Eqs 3.1-3.2 for code-phase, R_p , and carrier-phase, Φ_L , measurements show that both of them infer a slant range, ρ , with the rest being error sources that need to be estimated and removed. Notice that notation of instrumental delays and

multipath in carrier-phase is the lower-case equivalent of the code-phase.

$$R_P = \rho + \underbrace{c(dt_r - dt^s)}_{\text{clock bias}} + \underbrace{T}_{\text{troposphere}} + \underbrace{\alpha_f STEC}_{\text{ionosphere}} + \underbrace{K_{P,r} - K_{P^s}}_{\text{receiver \& satellite instrumental delays}} \quad (3.1)$$

$$+ \underbrace{M_P}_{\text{multipath}} + \underbrace{\epsilon_P}_{\text{random noise}}$$

$$\Phi_L = \rho + c(dt_r - dt^s) + T - \alpha_f STEC + k_{L,r} - k_{L^s} + \underbrace{\lambda_L N_L}_{\text{phase ambiguity}} + \underbrace{\lambda_L w}_{\text{phase windup}} \quad (3.2)$$

$$+ m_L + \underbrace{\epsilon_L}_{\text{random noise}}$$

There are at least two frequencies on which GNSS transmitters emit signals. This allows for the existence of multiple carrier- and code-phase observables. Different linear combinations between two frequencies can be used to remove error sources. One example is the linear combination which eliminates the ionospheric delay

$$R_C = \frac{f_1^2 R_{P1} - f_2^2 R_{P2}}{f_1^2 - f_2^2} = \rho + c(\delta t_r - \delta t^s) + T + M_C + \epsilon_C, \quad (3.3)$$

$$\Phi_C = \frac{f_1^2 \Phi_{L1} - f_2^2 \Phi_{L2}}{f_1^2 - f_2^2} = \rho + c(\delta t_r - \delta t^s) + T + B_C + \lambda_N w + m_C + \epsilon_C, \quad (3.4)$$

with $B_C = b_C + \lambda_N(N_1 + \frac{\lambda_W}{\lambda_2} N_W)$, where $\lambda_N = \frac{c}{f_1 + f_2}$, $\lambda_W = \frac{c}{f_1 - f_2}$ and $N_W = N_1 - N_2$. Note that terms containing the subscript C are $(\cdot)_C = \frac{f_1^2(\cdot)_1 - f_2^2(\cdot)_2}{f_1^2 - f_2^2}$. Further combination corroborates in the carrier-phase ambiguity resolution procedure.

Carrier-phase Ambiguity Resolution

Regarding carrier-phase measurements, the fractional phase difference between the incoming signal and the signal replica can be determined with great precision via the use of a numerically controlled oscillator in the receiver. The integer number of cycles, however, is an ambiguous term when a satellite first comes into view making the resolution of this ambiguity a necessary step in the estimation procedure.

As Eq. 3.2 shows, the main error sources are the tropospheric and ionospheric delay, the multipath and instrumental delays as well as the integer ambiguity term. Estimating or removing these error sources depends on whether one can gather quasi-independent information about them and formulate a properly defined estimation problem. The tropospheric delay, for example, which is dependent on the signal path, can be adequately defined at zenith, if there are visible satellites at different azimuth and elevation angles, i.e., at different paths. Equivalently,

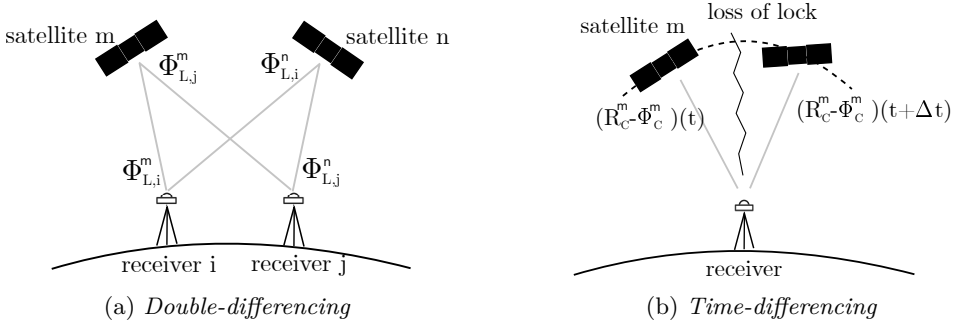


Figure 3.2: (a) The double-differencing (DD) technique is using two satellites and two receivers to allow determining integer ambiguities. (b) In time-differencing (TD) a single pair of satellite and receiver is used, determining float ambiguities. See text for further details.

in order for the instrumental delays of satellites and receivers to be quantified, observables from multiple satellites and multiple receivers must be used. Linear combinations of that manner, through a process called double-differencing (DD) as shown in Fig. 3.2a, produce phase observables which are free of instrumental delays, making the determination of the integer ambiguity term possible. Indeed $\Phi_{L,ij}^m = \Phi_{L,i}^m - \Phi_{L,j}^m$ and $\Phi_{L,ij}^n = \Phi_{L,i}^n - \Phi_{L,j}^n$ have $k_{L,ij}^m$ and $k_{L,ij}^n$ as instrumental delays which represent approximately the same quantity and further differencing produces the desirable DD observable $\Phi_{L,ij}^{mn} = \Phi_{L,ij}^m - \Phi_{L,ij}^n$ free of these biases. Multiple procedures of retrieving the integer term based on this concept have been developed (Teunissen et al., 2002).

An alternate route would be to not attempt fixing the ambiguities at their physical integer value. Treating them as floats implicitly means two possibilities, either (a) the ambiguity term is not confined to the integer space in the estimation problem containing the DD observables, or (b) the estimation problem is not constructed using DD observables at all. The latter means that one can use the raw measurements or more commonly the ionosphere-free linear combination in the time-differencing procedure. Under this regime, as shown in Fig. 3.2b, the evolution of geometry-free linear combination, $R_C - \Phi_C$, is monitored, and discovered discrepancies between subsequent time epochs are quantified to determine the magnitude of the float ambiguity. The precise positioning determination of a single receiver can be achieved, using just its own data, without the need to resort to the interferometric nature of DD. The instrumental delays are not explicitly removed but instead they are incorporated in the float ambiguity term. This single-receiver estimation process is called Precise Point Positioning (PPP). Lately, there has been development in combining this technique with global solutions to derive integer ambiguities (Geng et al., 2010; Laurichesse et al., 2009).

3.2 Receiver Clock Treatment

The signal which is emitted from the satellite consists of a carrier wave, modulated by the navigation message and a spread-spectrum technique so that the final signal has a unique time-dependent form. The signal replica is produced at the receiver in a similar fashion. For the two signals to be perfectly aligned, it would mean that the internal clocks of the receiver and the satellite need to be perfectly synchronised, which is never the case. It is this discrepancy between internal time-keeping mechanisms of space-based and ground-based segments of the system that produces a relative clock bias, $(dt_r - dt^s)$, as Equation 3.1 shows. Notice that this term contains dt_r which corresponds to the difference between receiver-kept time and true time, and dt^s which corresponds to the difference of the satellite-kept time and true time. Information about dt^s can be found either in the navigation message or in precise timing products obtained directly by IGS. This in turn disentangles the two quantities and allows for the determination of dt_r , i.e., the clock stability of the receiver clock. It is thus evident that any imperfection in the definition of the satellite clock is reflected on the behavior and the definition of the receiver clock. This highlights the importance of acquiring high-quality clock products especially if the subsequent estimation procedure is dependent on approximating the behavior of the clock via a stochastic process, which demands adherence to strict clock definitions.

Another important realisation is that linear combinations alter said definitions. The ionosphere-free observable contains $\delta t = (\delta t_r - \delta t^s)$, which is an “ionosphere-free” clock term with potentially different stability characteristics than the one from the raw measurements. Clock terms can be further augmented with, e.g., the instrumental delays of satellites and receivers which, since they are different for code- and carrier-phase, result in a so-called decoupled clock model with separate code and phase clocks (Collins et al., 2008). Notice also that the receiver clock bias cannot be meaningfully estimated if its value is lower than the noise level of the measurements. For these reasons, one cannot expect different definitions of GNSS receiver clocks to consistently behave approximately the same as the nominal one. An example of different clock behaviors due to these effects is shown in Fig. 3.3. While the “ionospheric-free” clock is used in all of them, the stability characteristics vary, from being close to nominal clock stability of an H-maser, as seen for the Matera clock, to showing large discrepancies, as seen for the other three example clocks.

3.3 GNSS in Space Geodesy

Code- and carrier-phase observables as shown in eqs 3.1-3.2 contain a slant range parameter, ρ . This is equal to the euclidean norm of the vector between satellite and receiver positions, \vec{p}^s and \vec{p}_r

$$\rho = \|\vec{p}^s - \vec{p}_r\|. \quad (3.5)$$

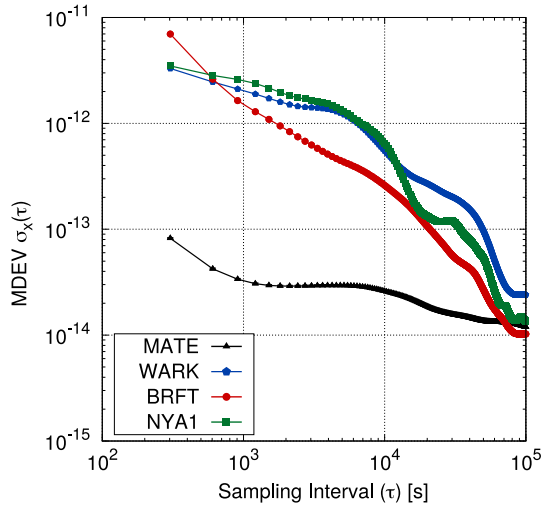


Figure 3.3: Modified Allan Deviation (MDEV) for four different GNSS receiver clocks during the CONT17 campaign. BRFT stands for Fortaleza, WARK for Warkworth, MATE for Matera, and ZECK for Zelenchukskaya.

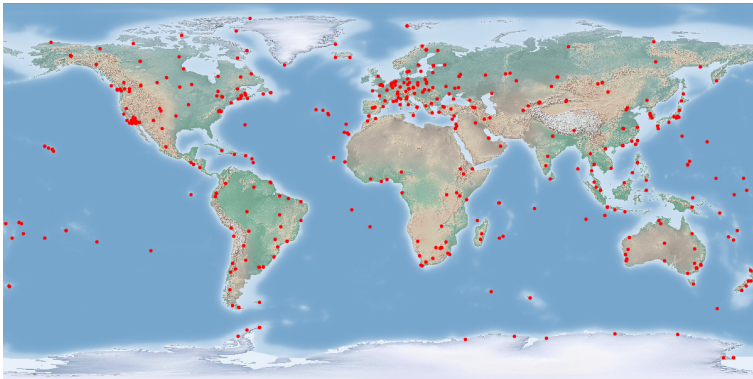


Figure 3.4: The network of GNSS stations contributing to the International GNSS Service (IGS) (Kouba, 2009).

The slant range observable, ρ , as shown in Eq. 3.5 is the norm of the vector difference and thus insensitive to the choice of reference frame. If a celestial reference frame were to be used, then a transformation of Earth-fixed satellite and receiver positions to that frame would need to take place, revealing the dependence of the observed slant range on EOP. The differential nature of this observable also shows that the precision of geodetic positioning of the ground-based segment is dependent and bounded by the precision of the space-based segment. The latter is in turn influenced by the presence of systematic errors which need to be estimated and removed. Common such errors are, e.g., the deficiencies in the models for gravitational and non-gravitational forces acting on the satellite orbits, or the presence of phase-center offsets of the satellite antennas that can be calculated after establishing a satellite-fixed nadir pointed reference frame.

It can be shown that (Rothacher et al., 1999)

$$\begin{aligned}\Delta(UT1 - UTC) &= -(\Delta\Omega + \cos(i)\Delta u_0)/k, \\ \delta(\Delta\epsilon) &= \cos(\Omega)\Delta i + \sin(i)\sin(\Omega)\Delta u_0, \\ \delta(\Delta\psi)\sin(\epsilon_0) &= -\sin(\Omega)\Delta i + \sin(i)\cos(\Omega)\Delta u_0,\end{aligned}\tag{3.6}$$

where ϵ_0 is the mean obliquity with respect to the ecliptic plane, $\delta(\Delta\epsilon)$, $\delta(\Delta\psi)$ are the celestial pole offsets in obliquity and in longitude respectively, and k is the ratio between universal and sidereal times. The orbital parameters Ω , i and u_0 are defined in Sec. 2.1. When one refers to GNSS as unable to give access to certain EOP directly, namely $UT1$ and celestial pole offsets, it means that they cannot be separated from the systematic errors of the orbits themselves. This collinearity is manifested in Eq. 3.6, where the orbital elements and the aforementioned EOP are almost linearly dependent. The common way to mitigate this issue, is to estimate the time-derivative of those EOP that exhibit this behavior, or to tightly constraint the chosen datum of the respective EOP in the estimation process.

The small size and the simple design of GNSS antennas and receiver systems have facilitated the establishment of numerous permanent GNSS stations in a densified global network. The network of GNSS stations contributing routinely to the International GNSS Service (IGS) is shown in Fig. 3.4. The global distribution and ubiquity of these stations has a positive impact on the quality of space-geodetic products as it increases sensitivity to determining parameters of interest. An example of this is shown in Fig. 3.5, where the analysis of PM from the Center for Orbit Determination in Europe (CODE) is carried out (Dach et al., 2013). The contributions of IGS, therefore, have become vital with respect to the maintenance of ITRF, PM and LOD products (Altamimi and Collilieux, 2009).

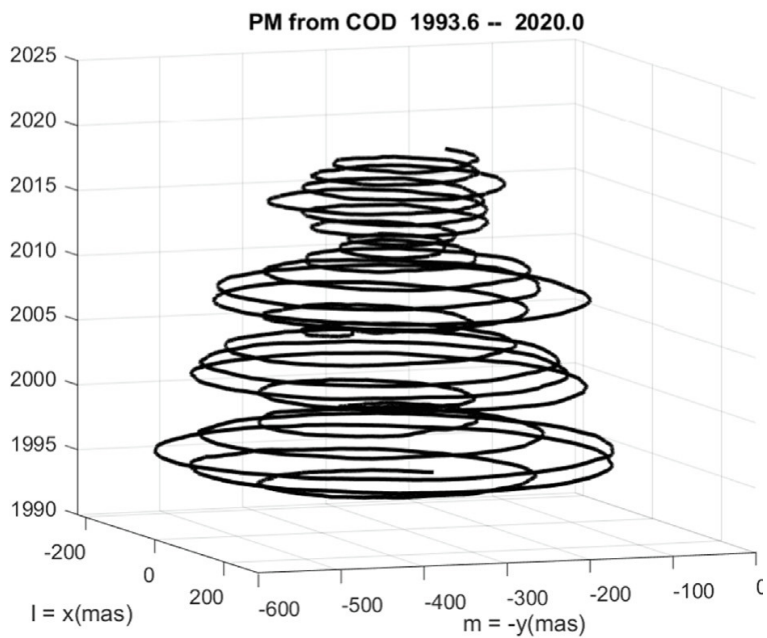


Figure 3.5: *GNSS-derived results covering for polar motion from 1993 to 2020 (Beutler et al., 2020).*

Chapter 4

Very Long Baseline Interferometry

Radio interferometry developed as a concept in the early 60's in the attempt to characterize and study distant active galactic nuclei called quasars (Sovers et al., 1998). The precision required for such a task cannot be attained by single radio telescopes as their angular resolution, at a given frequency, is inversely proportional to, and constrained by the antenna diameter. For this reason, a technique was developed so that multiple separated antenna elements can be used increasing the effective diameter and gaining access to higher resolutions. The process behind it is based on constructive and destructive interference between waves of the same frequency. Two antennas that are physically separated but observe the same source, record coherent signals albeit with a time-delay. Through the process of correlation and as a result of constructive interference, this time-delay can be extracted. Since different sources are located in different points in the sky, the time-delay is unique for each of them and thus gives information about their position with respect to the baseline that the two antennas form. When this expands into a network of stations, the correlation between time-delays and baselines can be mitigated allowing for the determination of the source positions.

The concept was first demonstrated over relatively small distances (on the order of 1 km) in the form of the a connected element interferometer, where antennas can be connected to the same clock and the correlation can be performed in real-time (Preston et al., 1983). The evolution and increased stability of frequency standards, with the advent of the atomic clock, and of recording equipment, diminished the need for this partial connection between different elements of the interferometer. Instead, interferometers were constructed in a complete separate manner over long (on the order of hundreds to the low end of thousands of km) and very long distances (Whitney et al., 1976) resulting in so-called Very Long Baseline Interferometry (VLBI). The determination of precise source positions is vital for their subsequent study and lies within the field of astrometric VLBI, while the (inverse) procedure of observing a well-defined catalogue of source positions in order to define station positions is a goal of geodetic VLBI. The International VLBI Service (IVS) is the governing body for the upkeep and dissemination of high quality space-geodetic products derived from VLBI observations (Nothnagel et al., 2017).

4.1 Basic VLBI Observables

A simple two-element interferometer is presented in Fig. 4.1. A distant point-like source is emitting electromagnetic waves that arrive in a planar front at the receiving stations. The received signals, undergo amplification, downconversion and formatting before being recorded and sent to the correlation centres. The objective is to attain the main observable, the time-delay τ_d , which is predominantly attributed to the geometry between the receiving stations and the source. It can, therefore, be approximated by

$$\tau_d = -\frac{1}{c} \vec{s} \cdot \vec{b}, \quad (4.1)$$

where \vec{s} and \vec{b} , are the source and baseline vector, respectively, expressed in the GCRS. Using Eq. 2.1, the baseline vector can be transformed to the ITRS equivalent meaning that the VLBI observables can be used to infer EOP. The signals in GNSS are transmitted at specified frequencies, show good signal-to-noise ratio (SNR) and their form, unmodulated by error sources like atmospheric refraction, is completely known to the receiver. The signals received by VLBI are weak and can be approximated best as band-limited white noise. This makes the process of determining the group and phase delays more challenging.

4.1.1 Correlation

The process of correlation can be described as follows. The signals, $u_1(t)$ and $u_2(t)$, (treated as continuous-time functions) are time-shifted with respect to each other, multiplied and averaged, i.e.,

$$\mathcal{R}(\tau) = \int_T u_1(t)u_2(t - \tau)dt, \quad (4.2)$$

where T is the integration time. Any choice of τ that causes the two signals to still be misaligned, leads to the multiplication generating another random signal and the subsequent integration averages it out. There exists, therefore a τ , which maximizes the value of \mathcal{R} and corresponds to the observed time-delay. Using Fourier transformation of Eq. 4.2, the (angular) frequency-dependent cross-power spectrum of the two signals can be obtained as

$$S_{u_1 u_2}(\omega) = A(\omega)e^{i\Phi(\omega, t)}, \quad (4.3)$$

where for a reference angular frequency ω_0 and reference time t_0

$$\Phi(\omega, t) = \Phi_0(\omega_0, t_0) + \frac{\partial\Phi}{\partial\omega}(\omega - \omega_0) + \frac{\partial\Phi}{\partial t}(t - t_0), \quad (4.4)$$

with $\tau_g = \frac{\partial\Phi}{\partial\omega}$ the group delay, and $\Phi_0(\omega_0, t_0)$ a phase ambiguity term. The different effects that dominate the correlation process can be seen in Eq. 4.4, namely the delay-rate term which corresponds to the diurnal motion of the source with respect

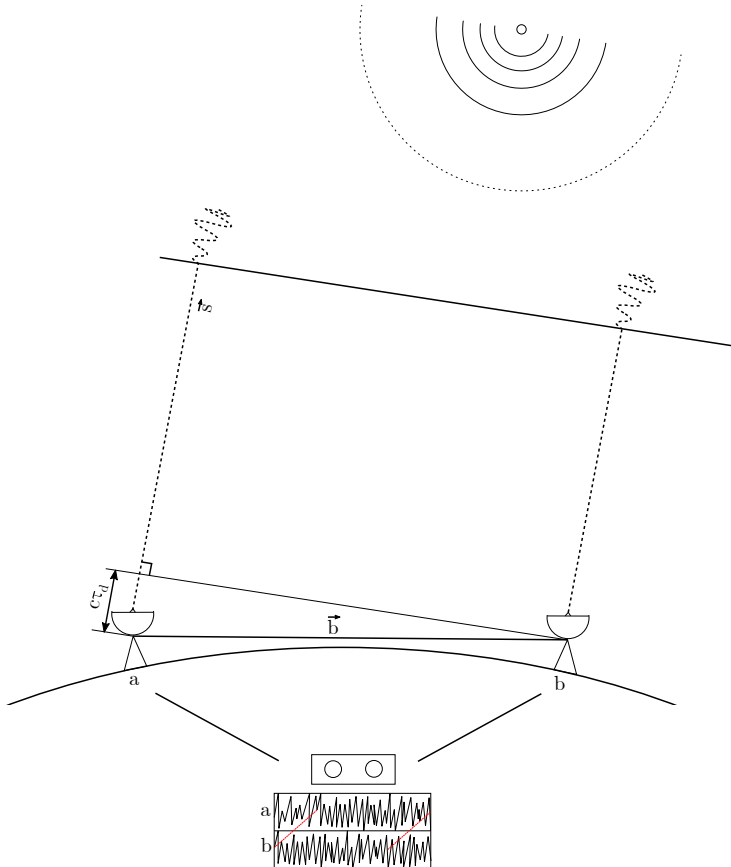


Figure 4.1: *The geodetic concept of VLBI observations. A planar wave front emitted from a distant radio source is received at two stations forming a baseline. The signals are recorded and subsequently correlated to extract the time-delay by matching the common patterns.*

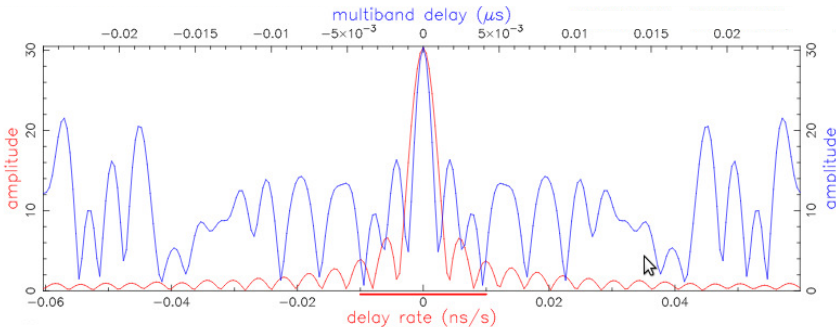


Figure 4.2: The residual multi-band delay and delay-rate for an X-band observation between the 20 m legacy telescope and one of the new generation VLBI Global Observing System (VGOS) telescopes, at Onsala (Sweden). The fringe-fitting has been carried out with the fourfit software (Cappallo, 2017).

to the baseline, and the frequency-dependent term which if too high will cause the so-called fringe pattern at the correlator output to oscillate rapidly impeding the correlation process. It is thus desirable to use an a priori guess of the group delay, τ_i , calculated through the delay model, and subtract it from the group delay $\delta\tau_g = \tau_g - \tau_i$, as well as an estimate of the delay-rate term in the same manner, to reduce Eq. 4.4 to the residual fringe phase defined as

$$\Delta\Phi(\omega, t) = \Phi_0(\omega_0, t_0) + \delta\tau_g(\omega - \omega_0) + \Delta\frac{\partial\Phi}{\partial t}(t - t_0), \quad (4.5)$$

with the residual group delay $\delta\tau_g$ and the the residual delay rate, $\Delta\frac{\partial\Phi}{\partial t}$. This is an effective way of reducing the search window during correlation. Substituting the residual fringe phase into Eq. 4.5 and performing an inverse Fourier transformation reveals the fringe pattern. In particular, the latter takes the form of $A \cos \Delta\Phi$ where $\Delta\Phi$ is principally driven by the residual group delay and delay rate. Thus, correct resolution and compensation lead to it maximizing and producing a fringe pattern, as shown in Fig. 4.2. Since the VLBI signal is weak, travelling through the signal chain can distort it enough so that the correlation process is unsuccessful. For this reason, the fringe fitting process has to account for instrumental delays as well. The principal way of tackling this issue is to inject a signal of known phase before the LNA and measure the phase shift (phase-cal).

After the residual fringe phase, group delay and delay-rate have been established, they are added to the instrumental delays used in order to get the total values and hence the three observables, namely the delay-rate $\frac{\partial\Phi}{\partial t}$, the group delay $\frac{\partial\Phi}{\partial\omega}$ and the fringe phase $\Phi(\omega, t)$. Note that the latter contains the cycle ambiguity which prevents from it being used in a straightforward manner. The determination of the time-delay per frequency channel gives what is known as single-band delay (SBD). After the SBDs have been obtained, a process of determining a common delay over all channels is carried-out, giving the multi-band delay (MBD). This is accomplished through the bandwidth synthesis technique (Kondo and Takefuji,

2016; Shaffer, 2000). The uncertainty of the multi-band group delays is given as (Shaffer, 2000)

$$\sigma_{\tau_g} = \frac{1}{2\pi SNR f_{rms}}, \quad (4.6)$$

where f_{rms} is equal to the root mean square of the frequency span or 40 % of the total bandwidth.

Summarizing, the correlation process can be described as follows. The signal, collected in two stations forming a baseline, can be approximated as band-limited white noise. Such a characterisation means that one can think of it as a set S of monochromatic signals of different frequencies. A subset $S_s \subset S$ of them is what the source is emitting while the rest are noise. Through the process of correlation the signal of one station is shifted with respect to the reference station of the baseline, until the subsets S_s of the two signals align in time. This is accomplished when the cross-correlation of the signals maximizes, i.e., their multiplication and averaging removes the noise and amplifies the common patterns.

4.1.2 Scheduling

It is evident, looking at the characteristics of the correlation procedure, that a high SNR can be achieved for (a) long integration times which have a positive effect on averaging out noise, (b) large bandwidth which means more monochromatic components of the source signal. The value of SNR can be further augmented by the observation of point-like bright sources, low system noise and a large amount of channels. This is indeed true as (Shaffer, 2000),

$$SNR = \frac{\eta_c S_f}{\sqrt{SEFD_1 SEFD_2}} \sqrt{2B_{ch} N_{ch} T}, \quad (4.7)$$

where $SEFD$ is the system equivalent flux density and is related to system noise temperature of the receiving system normalised by the effective area of the antenna. S_f is the flux density of the radio source, η_c an efficiency factor for sampling and correlation, while N_{ch} and B_{ch} are the number of channels and channel bandwidth respectively. The need arises, when talking about an interferometric network of stations, for scheduling that optimizes for the aforementioned parameters. Since the networks need to have a worldwide distribution, it might mean that subnets of stations are formed during the observation process. For geodetic VLBI experiments, schedules are produced by specialised software, namely *Sked* (Gipson, 2010) and *VieSched++* (Schartner and Böhm, 2019) which output so-called *.skd* files. The files contain not only the observation schedule but also the sampling mode, and the frequency channel setup, i.e., bandwidth number of channels and center frequency per band.

4.2 VLBI Delay Model

The delay as expressed in the simplified form of Eq. 4.1 is augmented with the influence of certain physical phenomena. The change of the ray path due to the

gravitational attraction that it experiences as it passes by of our solar system must be accounted for. The general relativistic term added to the simple delay model is

$$\Delta T_{grav} = \sum_j \Delta T_{grav_j}, \quad (4.8)$$

where j refers to a specific gravitational body (Petit and Luzum, 2010)

$$\Delta T_{grav_j} = 2 \frac{GM_j}{c^3} \ln \frac{|\vec{R}_{1j}| + KR_{1j}}{|\vec{R}_{2j}| + KR_{2j}}, \quad (4.9)$$

with \vec{K} the unit vector from the barycenter to the source and R_{ij} the vector from j^{th} gravitational body to the i^{th} receiver. The latter are given for a single baseline as (Petit and Luzum, 2010)

$$\begin{aligned} R_{1j} &= \vec{X}_1(t_1) - \vec{X}_j(t_{1j}), \\ R_{2j} &= \vec{X}_2(t_1) - \frac{V_{\oplus}}{c} \vec{K} \cdot \vec{b} - \vec{X}_1(t_{1j}). \end{aligned} \quad (4.10)$$

It follows that in the case of Earth, these vectors correspond to the geocentric vectors, i.e., the coordinates expressed in the GCRS. The barycentric coordinates of a receiver i can be retrieved by a simple translation of the origin from the geocenter to the barycenter (Petit and Luzum, 2010)

$$\vec{X}_i = \vec{x}_i(t_1) + \vec{X}_{\oplus}(t_1), \quad (4.11)$$

while t_{1j} is equal to

$$t_{1j} = \min \left[t_1 - t_1 \frac{\vec{K} \cdot (\vec{X}_j(t_1) - \vec{X}_1(t_1))}{c} \right]. \quad (4.12)$$

The geocentric delay due to geometry, in vacuum, can be expressed as (Petit and Luzum, 2010)

$$t_{v2} - t_{v1} = \frac{\Delta T_{grav} - \frac{\vec{K} \cdot \vec{b}}{c} \left[1 - \frac{(1+\gamma)U}{c^2} - \frac{|\vec{V}_{\oplus}|^2}{2c^2} - \frac{\vec{V}_{\oplus} \cdot \vec{w}_2}{c^2} \right] - \frac{\vec{V}_{\oplus} \cdot \vec{b}}{c^2} (1 + \vec{K} \cdot \vec{V}_{\oplus}/2c)}{1 + \frac{\vec{K} \cdot (\vec{V}_{\oplus} + \vec{w}_2)}{c}}, \quad (4.13)$$

where U is the gravitational potential at the geocenter, neglecting Earth's mass. The delay term should include the geometric atmospheric effect visible in Fig. 2.2b and corresponding to the G term in Eq. 2.4 and given as (Petit and Luzum, 2010)

$$t_{g2} - t_{g1} = t_{v2} - t_{v1} + \delta t_{atm1} \frac{\vec{K} \cdot (\vec{w}_2 - \vec{w}_1)}{c}. \quad (4.14)$$

In conclusion the delay model is

$$\tau_d = t_{g2} - t_{g1} - t_{clk} - t_T - t_I - t_{misc}, \quad (4.15)$$

containing further the clock offsets, t_{clk} , the non-geometric term of the atmospheric refraction, t_T referring to the troposphere and t_I to the ionosphere. Miscellaneous error sources like the misalignment of the lateral displacement of the two principal axes of rotation of a telescope in a X/Y mount or the thermal and gravitational deformation of the antennas which result in additional delays (Nothnagel et al., 2019; Nothnagel, 2009; Wresnik et al., 2007) represented by t_{misc} . This term also includes errors induced by the frequency-dependent positional variation of radio sources, an outcome of their non-perfectly point-like nature (Anderson and Xu, 2018). Better modelling of effects that contribute to t_{misc} , like that of galactic aberration (MacMillan et al., 2019), help resolve them and produce a more robust delay model.

4.3 Data Analysis

The troposphere and the ionosphere can be modelled and estimated as discussed in Sec. 2.3. For the legacy VLBI systems the existence of two bands (S/X) makes it possible to obtain the ionospheric-free linear combination reflecting the similar process that happens in GNSS as shown in Eq. 2.6. The differential nature of the observables means that during data analysis a clock datum must be established and offsets with respect to this datum must be calculated. In addition, for the determination of station positions of a VLBI network, in a routine least-squares (LSQ) fit, an observation equation

$$A \cdot x = y, \quad (4.16)$$

where A is an $n \times m$ matrix linking, n observations to m estimable parameters. A set of normal equations (NEQ) is constructed of the form

$$N \cdot x = b, \quad (4.17)$$

where $N = A^T P A$ is an $m \times m$ so-called normal matrix and $b = A^T P y$, and P the variance-covariance matrix.

4.3.1 Datum Constraints

The matter of fact is that when solving for station positions and EOP there exists a rank deficiency in the normal matrix of Eq. 4.17. This means that not all parameters are linearly independent with respect to each other, which is motivated by the differential nature of interferometric measurements. In other words, VLBI analysis realises a frame which, unless some form of constraining is applied, lacks information on the position of its origin, when solving for station positions only, and also of how it is oriented when additionally estimating EOP. The solution should be that the estimated realisation of the frame must be constrained to an a priori one. This can be done by either fixing stations to their a priori positions, constraining the estimated correction to the a priori coordinates, a free-net solution, or by applying the minimal set of constraints needed so that the rank deficiency is

accounted for. The latter approach is called Minimal Constraints (MC). The MC approach seeks to nullify the Helmert transformation parameters between the two realisations of the frame. In particular, the estimated coordinates $(\tilde{x}_1, \tilde{y}_1, \tilde{z}_1, \dots, \tilde{z}_n)$ are related to the a priori coordinates, $(x_1, y_1, z_1, \dots, z_n)$, through the following similarity transformation (Sillard and Boucher, 2001)

$$\begin{pmatrix} \tilde{x}_1 \\ \tilde{y}_1 \\ \tilde{z}_1 \\ \vdots \\ \tilde{z}_n \end{pmatrix} = \begin{pmatrix} x_1 \\ y_1 \\ z_1 \\ \vdots \\ z_n \end{pmatrix} + \begin{bmatrix} 1 & 0 & 0 & x_1 & 0 & -z_1 & -y_1 \\ 0 & 1 & 0 & y_1 & z_1 & 0 & x_1 \\ 0 & 0 & 1 & z_1 & y_1 & -x_1 & 0 \\ \vdots & & & & & & \\ 0 & 0 & 1 & z_n & y_n & -x_n & 0 \end{bmatrix} \cdot \begin{pmatrix} T_x \\ T_y \\ T_z \\ s \\ R_x \\ R_y \\ R_z \end{pmatrix}. \quad (4.18)$$

Since it is a linear relation with respect to the three translation parameters T_x, T_y, T_z , the three rotation parameters R_x, R_y, R_z , and the scale parameter s , as evident in Eq. 4.18, the partial derivatives can be acquired in a straightforward way. They can be then appended on the otherwise singular matrix N so that the augmented matrix does not have rank deficiency (Altamimi et al., 2002). The resulting constraints are called no-net-translation (NNT) for nullifying the translation parameters, no-net-rotation (NNR) for nullifying the rotation parameters and no-net-scale (NNS) for nullifying the scale parameter. The advantage of this technique with respect to the others is that it retains information on the estimable characteristics of the geodetic network without deforming the geometry as defined by the observations. Different methods can be applied to mitigate a poor choice of an a priori frame, referred to as datum noise, or poor quality of observations, i.e., data noise (Kotsakis, 2018).

4.3.2 Parameter Constraints

Augmenting the normal matrix N of Eq. 4.17 with additional constraints is not limited to defining a geodetic datum. Data gaps that may appear due to downtime in one or multiple VLBI stations, increased radio frequency interference (RFI) in one or several observing channels, discontinuities in the clock parameters introduced at the correlation stage to facilitate fringe pattern extraction, lead to singularities in the LSQ formulation. Constraining the unresolvable parameters of interest, helps mitigate these issues and is usually done either on themselves or their rates. The constraints are input as pseudo-observations and the normal matrix is augmented to accommodate for the new dimensionality (Artz et al., 2016).

4.4 VLBI in Space Geodesy

VLBI is the only technique in Space Geodesy that observes extragalactic sources and as such, it can have access to all EOP. This has made it an invaluable contributor to high quality space-geodetic products. Observations usually span 24 hours, and the quality of their products dependent on the polyhedron the observing network

is covering (Malkin, 2009). Examples of geodetic VLBI sessions that are organised regularly by IVS are:

- The *IVS-R1* and *IVS-R4* sessions that take place two times per week and are comprising of a modest set of 7-9 stations and are designed to be used for EOP estimation.
- The intensive (*Int*) sessions on baselines, Wettzell (Germany) to Kokee Park (USA), called *Int1*, and Wettzell (Germany) to Ishioka (Japan) called *Int2*, which aim at $UT1 - UTC$ and last 1 hour. There is also an intensive series network comprising of Wettzell (Germany), Ishioka (Japan) and Ny-Ålesund (Norway). Due to the unpredictable nature of $UT1 - UTC$, the measurements are taken daily.
- The *IVS-T2* sessions aiming at TRF which comprise of a more populous network of 14-18 stations and take place at least twice a year.
- The two week continuous VLBI observations, *CONT* sessions, involving a comprehensive network with the largest volume of polyhedron formed. These measurements aim at the utmost accuracy that VLBI can offer.
- The *R&D* sessions which take place every month and aim to investigate and study instrumental effects and product improvement.

Chapter 5

Combination of Space-geodetic Techniques

Space-geodetic techniques, apart from positioning determination, can be used for the definition of reference frames through the determination of their origin, orientation and scale. A single technique, however, cannot uniquely define a frame. In the case of the ITRF (Altamimi et al., 2016), the origin of the frame, i.e., the geocenter is primarily accessed through SLR. The scale parameter is determined from both VLBI and SLR, and the orientation is defined through an MC approach incorporating observations from all four techniques with respect to previous realisations of the ITRS. It is evident, therefore, that for a proper frame definition, a combination of multiple space-geodetic techniques is essential.

Even when the primary goal is not the realisation of a reference system, the simultaneous processing of multiple techniques facilitates the transfer and the increase of frame information among them, like, e.g., access to SLR-derived geocenter by GNSS (Thaller et al., 2011). The concept of co-location sites, i.e., sites which contain several space-geodetic instruments (stations) becomes crucial in this context since, these stations share frequency standards in the form of common clocks and feature similarity in atmospheric refraction phenomena. Combination featuring these sites leads to an improvement in, e.g., inter-continental frequency transfer (Hobiger et al., 2015) and in overall quality of parameters of interest like station positioning or EOP through the better resolution of tropospheric delays (Krügel et al., 2007). Combined networks allow for the densification and better geometry of the attained observation set and ensure overall robustness since common parameters are simultaneously inferred from independent techniques. The latter, especially, helps with mitigating technique-specific biases, like e.g., mismodelling of phase center correction for GNSS antennas and the effect it has on tropospheric delay determination (Ejigu et al., 2019). Ultimately, by the application of common displacement models and simultaneous determination of common parameters of interest, combination allows for consistency and homogeneity in the problem formulation which benefits the precision and quality of space-geodetic products.

5.1 Combination Strategies

Three main strategies are used when attempting a combination of multiple space-geodetic techniques, namely (a) combination on the results level, (b) combination on the normal equation level and (c) combination on the observation level.

5.1.1 Combination on the Results Level

Combination on the Results Level (CRL) is routinely employed for the successive iterations of the ITRF(Altamimi et al., 2011, 2016; Boucher et al., 2004). In the context of frame definition it works as follows. Single-technique solutions which span several years of data are carried out at first and time series of station positions, velocities and EOP are generated. The produced results are then input into a combined problem which contains a 14-parameter similarity transformation, similar to the Helmert transformation presented in Eq. 4.18 in Sec. 4.3.1, but expanded to the rates of the translation, rotation and scale parameters. In the formulated problem at this second stage, all single-technique acquired parameters are used as observations with a combined solution analog being produced as a result. In this strategy, as station positions and EOP are first computed independently, there is no possibility of capitalising on commonalities in co-location sites, like frequency standards or atmosphere. The convergence points between the different techniques are instead (a) the common frame-defining parameters, (b) the common EOP and (c) the existence and utilisation of so-called local ties (LT), elaborated in Sec 5.2, at co-location sites. The single-technique time-series undergo a pre-combination process where they are evaluated in the context of the velocity fields they produce between adjacent stations, enabling for their homogenisation and outlier removal. The latest iterations of this technique also include post-seismic as well as displacement models and modelling and mitigation of seasonal variations on the station position signal caused by geophysical loading phenomena or system-specific biases like, e.g., draconitic periods of satellite orbits in GNSS (Altamimi et al., 2016; Griffiths and J. R. Ray, 2013).

5.1.2 Combination on the Normal Equation Level

The single-technique analysis step before the main combination which is present in CRL, gives the ability to the analyst to evaluate these interim results and to remove discontinuities or irregularities. On the other hand, this process does not take into account some important information that stems from the common error sources at co-location sites. The correlation between these error sources and parameters of interest is invariably lost along with what better resolution of them demonstrably offers (Hobiger and Otsubo, 2015). Combination on the Normal Equation Level (CNL) has been developed to mitigate this issue. In this approach, the following steps are performed, namely (a) a set of datum-free NEQ is constructed for each technique which are then, (b) modified by pre-eliminating parameters that correspond to error sources, (c) put together through the process of so-called stacking, and (d) append datum information using an approach like

MC (Thaller, 2008). Starting from the Eq. 4.17, the process of pre-elimination is splitting the normal matrix N between parameters of interest x_1 and nuisance parameters x_2 as

$$\begin{bmatrix} N_{11} & N_{12} \\ N_{21} & N_{22} \end{bmatrix} \begin{pmatrix} x_1 \\ x_2 \end{pmatrix} = \begin{pmatrix} b_1 \\ b_2 \end{pmatrix}, \quad (5.1)$$

which is essentially a system of two linear equations,

$$\begin{aligned} N_{11} \cdot x_1 + N_{12} \cdot x_2 &= b_1, \\ N_{21} \cdot x_1 + N_{22} \cdot x_2 &= b_2, \end{aligned} \quad (5.2)$$

where x_2 can be eliminated by a linear combination of the system resulting in the reduced expression

$$(N_{11} - N_{12}N_{22}^{-1}N_{21}) \cdot x_1 = b_1 - N_{12}N_{22}^{-1} \cdot b_2. \quad (5.3)$$

So CNL, in contrast to CRL, through the construction of a unified set of normal equations, retains the essential information and correlations between the target parameters and those which pertain to error sources allowing for the combination approach to fully exploit this trait for stations that are co-located.

5.1.3 Combination on the Observation Level

The Combination on the Observation Level (COL) is close in definition to CNL as it can be approached by means of constructing and stacking NEQ. The main differences lie firstly in the fact that COL lacks a pre-elimination process which means that all technique-specific parameters are reachable by the analyst (Biancale et al., 2010). And secondly, in the consistency and homogeneity of the a priori information and models used and the historical development of data analysis using these techniques. In the absence of multi-technique space-geodetic softwares like, e.g., *c5++* (Hobiger et al., 2010), the analysis centres construct a technique-specific set of datum-free NEQ as a first step in a two-step process. Then, these equations are sent to the combination centres, where CNL is performed. The ability to analyze several space-geodetic observables within one software package means that the generation and process of combined NEQ can be done in one step, ensuring the highest level of consistency between them (Artz et al., 2012; Thaller, 2008). In this context, in paper I, a COL was attempted using VLBI and GNSS in inter- and intra-technique modes to evaluate TRF and EOP products. The GNSS and VLBI were linked without local ties but via common atmosphere, while two VLBI networks are linked with common EOP. More details follow in Sec. 6 (Diamantidis et al., 2020).

5.2 Local Ties

The combination strategies essentially seek to find and exploit commonalities between the different space-geodetic techniques. In CRL, in particular, where

single-technique solutions provide a set of station positions, velocities and EOP, it is evident that each technique generates its own frame definition. The objective of combination in this sense is to find an “optimum” average of these. While the same applies for EOP, this is not the case for station positions since they are inherently different. Additional observations that attempt to establish a link between station positions can, therefore, strengthen the combination procedure. This is what LT, i.e., a set of three dimensional measurements between stations at co-location sites, contribute. Despite the fact that LT are very precise and can reach millimeter level accuracy, discrepancies on the centimeter level can be detected between them and the ITRF-derived distances (Altamimi et al., 2016; J. Ray and Altamimi, 2005). Technique-specific error sources contribute also to discrepancies between LT and distances obtained through single-technique solutions (Nothnagel et al., 2019). The LT information is input as a pseudo-observation

$$\begin{pmatrix} x \\ y \\ z \end{pmatrix}_{tie} = \begin{pmatrix} x \\ y \\ z \end{pmatrix}_i - \begin{pmatrix} x \\ y \\ z \end{pmatrix}_j, \quad (5.4)$$

where i and j represent different stations at the same co-location site.

Proper evaluation and weighting of the LT is thus essential in order for them to contribute to the combination in an effective manner. The weighting is commonly done in an iterative empirical manner by either inspecting post-fit residuals (Altamimi et al., 2016) or by evaluating the effect of LT in the EOP estimation. Inspection of $UT1 - UTC$ estimates for a combination between VLBI and GNSS stations by incorporating different ties shows that beneficial tie information results in improved station position repeatabilities without affecting the mean correction of $UT1 - UTC$ estimates with respect to a priori values (Thaller, 2008).

5.3 A Novel Approach to Combination

As described in Sec. 5.2 LT are essential in providing an innate link between inherently different parameters like the positions of different stations at a co-location site. Ultimately, they need to be adjusted and weighted as they represent different optima from the positions derived through the means of Space Geodesy. While the latter are obtained from a global solution and represent the optimal values that provide the most stable frame definitions, tie measurements reflect the absolute precision at a local level. It is also evident by Eq. 5.4 that an attempt to estimate station positions utilizing only LT would result in a rank deficient problem.

These two realisations motivate a new strategy. The geometric link between stations at a co-location site becomes a primary parameter of interest instead of an aiding pseudo-observation in the combination process (Fig. 5.1). This means that a problem reformulation is carried out as follows. A station is chosen as the origin of the local vector, and it is the one that corresponds to the technique with the highest frequency of observations, i.e., GNSS, for reasons that will be explained

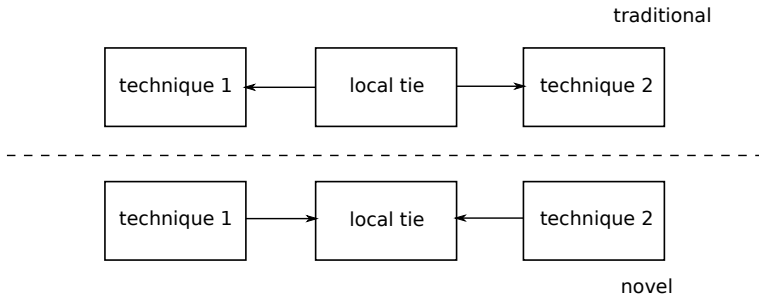


Figure 5.1: *Conceptual difference for the utilisation of local ties between traditional and novel techniques. The traditional technique estimates station positions of co-located stations augmenting the problem with local ties as independent measurements. The novel one estimates the common vector between co-located stations using local ties as measurements to directly observable parameters. Details are presented below.*

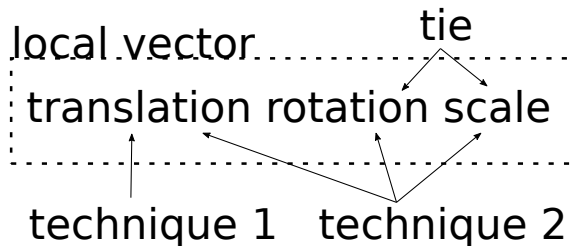


Figure 5.2: *The novel technique focuses on estimating the translation, rotation and scale of the local vector. While translation is linearly dependent to rotation/scale, this dependency is mitigated by a clear distinction of how the observations are used in the construction of the LSQ problem. The high-frequency first technique is driving the estimation of the translation parameter, while the local ties are used to clearly disassociate the rotation/scale parameters from it.*

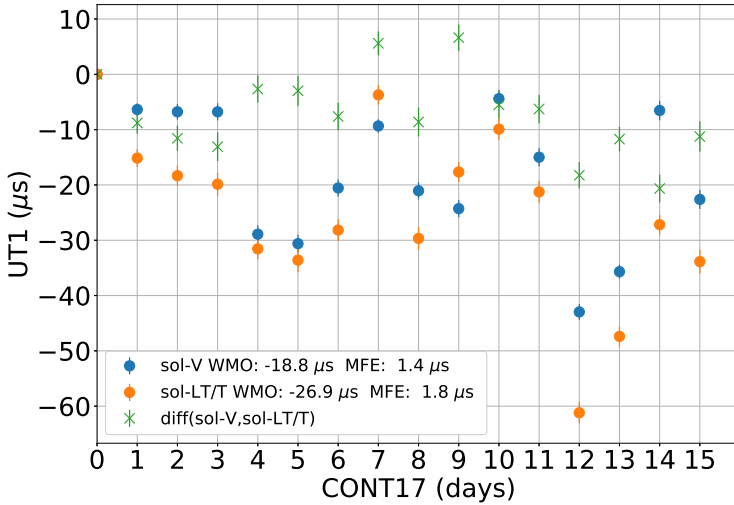


Figure 5.3: $UT1 - UTC$ comparison between single-technique (*sol-V*) and untuned *LT* traditional formulation (*LT/T*).

further. What would normally be the correction to GNSS station positions, now corresponds to the translation of the local vector. The second co-located technique is used to sense both the translation of this vector as well as its rotation and scale. The motivation behind this lies in the fact that rotation/scale of the local vector and translation of its origin are linearly dependent and artificially decoupling them is physically inconsistent, as in every iteration of the estimation procedure the point of the origin is the basis on which rotation/scale will be determined. The collinearity present is mitigated twofold and can be seen in Fig. 5.2. The translation of the local vector is simultaneously provided and primarily driven by the high-frequency technique, in this case GNSS, akin to a “high-low” configuration in sensor fusion. The rotation and scale are independently accessed through the local tie measurements. In particular, the a priori positions are used to calculate the (a priori) local vector which is compared to the one obtained from the *LT*, extracting equivalent “local tie” rotation and scale parameters. They are, then, utilised as pseudo-observations with respect to the estimated rotation R_x, R_y and scale s of local vector between stations i and j ,

$$\begin{pmatrix} R_x \\ R_y \\ s \end{pmatrix}_{tie} = \begin{pmatrix} R_x \\ R_y \\ s \end{pmatrix}_{ij}. \quad (5.5)$$

This constitutes a major departure in the utilisation of *LT*, since they are used to observe what they inherently are instead of the differential nature of two primary parameters of interest that Eq. 5.4 dictates.

The technique was tested during the continuous 15-day CONT17 VLBI campaign (Behrend et al., n.d.) for a COL between the VLBI and co-located GNSS stations

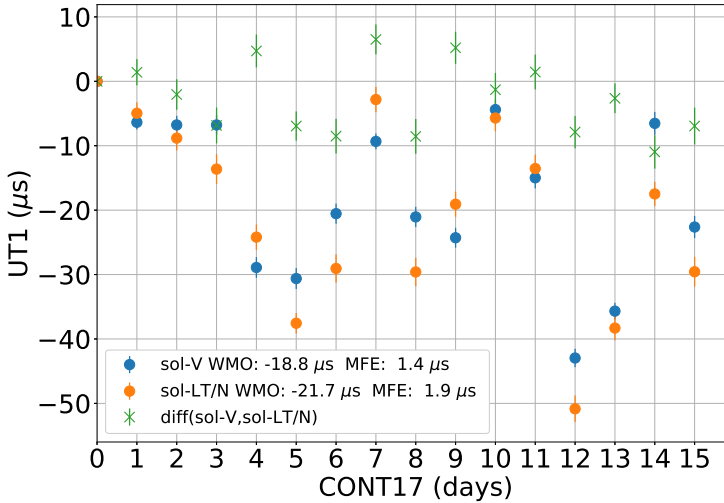


Figure 5.4: $UT1 - UTC$ comparison between single-technique ($sol-V$) and untuned LT novel formulation (LT/N).

using the `c5++` space-geodetic software. Common atmosphere was estimated and LT were used in the traditional and novel frameworks of formulating them. All but two ties were utilised and no empirical tuning was applied. The effect of the LT on $UT1 - UTC$ is used as a metric to quantify the homogenisation that each process provides and presented in Figs. 5.3-5.4. It is clear that the novel process results in mean biases on a comparable level to single-technique solutions, thus outperforming the traditional formulation. However, one can detect a bias in the form of larger uncertainties with respect to the single-technique solution indicating the need for some form of empirical tuning.

The robustness of the process is seemingly improved as well. Day 6 of CONT17 is a good candidate to test it due to multiple technical failures that resulted in data gaps for 8 out of the 14 stations of the VLBI network. In addition, co-located VLBI and GNSS stations in Zelenchukskaya exhibited multiple clock breaks. Overall, the analysis of this day is a typical example where additional constraints are needed, as described in Sec. 4.3, especially when it comes to clock offsets in order to retrieve EOP, given their close correlation. Using the same setup of loose constraints on the clock, on the order of 7.2 ns/h, the novel technique is able to retrieve reasonable EOP values while the traditional technique clearly diverges, as shown in Fig. 5.5. While more investigation is needed in order to quantify an improvement on the level of station position repeatabilities and to remove the residual bias from the estimated EOP parameters, the novel technique shows promise in further homogenising the combination process.

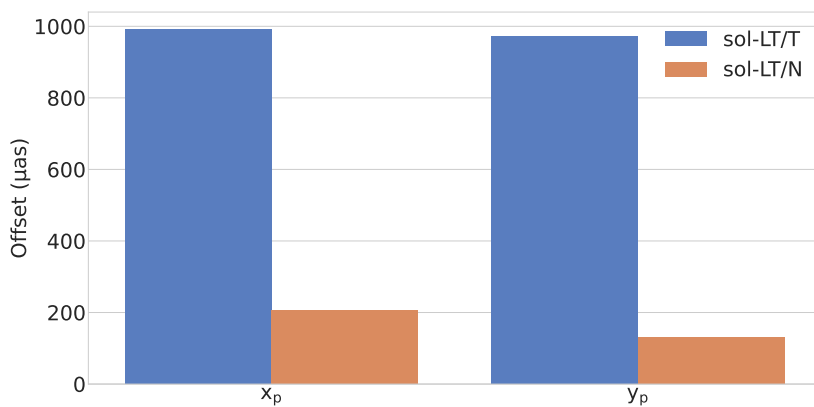


Figure 5.5: Offsets computed for PM components for day 6 of CONT17, for the traditional formulation (sol-LT/T) and the novel one (sol-LT/N).

Chapter 6

Summary and outlook

This thesis has presented general topics that are pertinent in any space-geodetic analysis along with the specific working principles of two space-geodetic techniques, VLBI and GNSS, their contributions to space-geodetic products and their role in the realisation of the ITRF. The concept of combination was then explored, looking at the different techniques used and their limitations with respect to LT utilisation. A novel approach for multi-technique combination was presented along with a proof of concept. Further work is needed to explore the concept in the form of optimal weighting techniques for LT so as to detect and quantify tangible in station positions. Finally, the work should expand in order to encompass the concept of co-location in space (Anderson et al., 2018) by incorporating and studying the topic of Precise Orbit Determination (POD) (Klopotek et al., 2020).

Summary of Paper I

The topic of COL was examined in two different ways, using the continuous VLBI campaign CONT17 as a dataset. Firstly, a COL on the level of common atmosphere between the Legacy-1 VLBI network that participated in CONT17 and the co-located GNSS stations, where the precision of derived station position was compared with respect to single-technique solutions. Secondly, the two legacy VLBI networks of CONT17 were combined on the level common EOP, and the accuracy of the derived PM, between the two combination schemes with respect to IGS products, was evaluated.

Bibliography

- Agnew, D. C. (2015). Earth Tides. *Treatise on Geophysics, Volume 3: Geodesy*, 151–178. DOI: 10.1016/B978-0-444-53802-4.00058-0.
- Altamimi, Z. and X. Collilieux (2009). IGS contribution to the ITRF. *Journal of Geodesy*, **83**(3-4), 375–383. DOI: 10.1007/s00190-008-0294-x.
- Altamimi, Z., C. Boucher, and P. Sillard (2002). New trends for the realization of the International Terrestrial Reference System. *Advances in Space Research*, **30**(2), 175–184. DOI: 10.1016/S0273-1177(02)00282-X.
- Altamimi, Z., X. Collilieux, and L. Métivier (2011). ITRF2008: an improved solution of the international terrestrial reference frame. *Journal of Geodesy*, **85**(8), 457–473. DOI: 10.1007/s00190-011-0444-4.
- Altamimi, Z., P. Rebischung, L. Métivier, and X. Collilieux (2016). ITRF2014: A new release of the International Terrestrial Reference Frame modeling nonlinear station motions. *Journal of Geophysical Research: Solid Earth*, **121**(8), 6109–6131. DOI: 10.1002/2016JB013098.
- Anderson, J. M., G. Beyerle, S. Glaser, L. Liu, B. Männel, T. Nilsson, R. Heinkelmann, and H. Schuh (2018). Simulations of VLBI observations of a geodetic satellite providing co-location in space. *Journal of Geodesy*, **92**(9), 1023–1046. DOI: 10.1007/s00190-018-1115-5.
- Anderson, J. M. and M. H. Xu (2018). Source structure and measurement noise are as important as all other residual sources in geodetic VLBI combined. *Journal of Geophysical Research: Solid Earth*, **123**(11), 10–162.
- Artz, T., L. Bernhard, A. Nothnagel, P. Steigenberger, and S. Tesmer (2012). Methodology for the combination of sub-daily Earth rotation from GPS and VLBI observations. *Journal of Geodesy*, **86**(3), 221–239. DOI: 10.1007/s00190-011-0512-9.
- Artz, T., S. Hallsig, A. Iddink, A. Nothnagel, and C. Tegtmeier (2016). “Constraining Least-Squares VLBI Solutions”. *International VLBI Service for Geodesy and Astrometry 2016 General Meeting Proceedings: “New Horizons with VGOS”*.

- Ed. by D. Behrend, K. D. Baver, and K. L. Armstrong. NASA/CP-2016-219016, pp. 193–197.
- Behrend, D., C. Thomas, J. Gipson, E. Himwich, and K. Le Bail (n.d.). On the organization of CONT17. *Journal of Geodesy* (). DOI: 10.1007/s00190-020-01436-x.
- Beutler, G., A. Villiger, R. Dach, A. Verdun, and A. Jäggi (2020). Long polar motion series: Facts and insights. *Advances in space research*, **66**(11), 2487–2515.
- Biancale, R., D. Gambis, and R. J.-Y. (Oct. 2010). *Why combining at the Observation Level?* https://www.iers.org/SharedDocs/Publikationen/EN/IERS/WorkingGroups/CombinationOL/REFAG2010_Biancale.pdf?__blob=publicationFile&v=1.
- Biggs, J., T. Wright, Z. Lu, and B. Parsons (2007). Multi-interferogram method for measuring interseismic deformation: Denali Fault, Alaska. *Geophysical Journal International*, **170**(3), 1165–1179. DOI: 10.1111/j.1365-246X.2007.03415.x.
- Boehm, J., B. Werl, and H. Schuh (2006). Troposphere mapping functions for GPS and very long baseline interferometry from European Centre for Medium-Range Weather Forecasts operational analysis data. *Journal of Geophysical Research: Solid Earth*, **111**(B2). DOI: 10.1029/2005JB003629.
- Boucher, C., Z. Altamimi, P. Sillard, and M. Feissel-Vernier (2004). *The ITRF2000 (IERS Technical Note)*. Vol. 31. Frankfurt am Main: Verlag des Bundesamts für Kartographie und Geodäsie, pp. 1–289. ISBN: 3-89888-881-9.
- Boy, J.-P., J. Hinderer, and P. Gegout (1998). Global atmospheric loading and gravity. *Physics of the Earth and Planetary Interiors*, **109**(3-4), 161–177. DOI: 10.1016/S0031-9201(98)00122-8.
- Brockmann, E., D. Ineichen, U. Marti, S. Schaer, A. Schlatter, and A. Villiger (July 2012). “Determination of Tectonic Movements in the Swiss Alps Using GNSS and Levelling”. *International Association of Geodesy Symposia*. Vol. 136, pp. 689–695. ISBN: 978-3-642-20338-1. DOI: 10.1007/978-3-642-20338-1_85.
- Capitaine, N. (2008). “Nomenclature and numerical standards for IAU models and IERS Conventions for Earth rotation”. *Proceedings of the Journées 2008 “Systèmes de référence spatio-temporels” X. Lohrmann-Kolloquium: Astrometry, Geodynamics and Astronomical Reference Systems*. Ed. by M. Soffel and N. Capitaine. Lohrmann-Observatorium and Observatoire de Paris, pp. 46–49. ISBN: 978-2-901057-63-5.
- Cappallo, R. (2017). *FOURFIT user’s manual*.
- Charlot, P., C. Jacobs, D. Gordon, S. Lambert, A. de Witt, J. Böhm, A. Fey, R. Heinkelmann, E. Skurikhina, O. Titov, et al. (2020). The third realization of the International Celestial Reference Frame by very long baseline interferometry. *Astronomy & Astrophysics*. DOI: 10.1051/0004-6361/202038368.

- Collins, P., F. Lahaye, P. Heroux, and S. Bisnath (2008). “Precise point positioning with ambiguity resolution using the decoupled clock model”. *Proceedings of the 21st international technical meeting of the satellite division of the Institute of Navigation (ION GNSS 2008)*, pp. 1315–1322.
- Dach, R., S. Schaer, S. Lutz, M. Meindl, H. Bock, E. Orliac, L. Prange, D. Thaller, L. Mervarta, A. Jäggi, G. Beutler, E. Brockmann, D. Ineichen, A. Wiget, G. Weber, H. Habrich, J. Ihde, P. Steigenberger, and U. Hugentobler (2013). “Center for Orbit Determination in Europe (CODE)”. *International GNSS Service, Technical Report 2012 (IGS Annual Report)*. Ed. by R. Dach and Y. Jean. IGS Central Bureau and University of Bern, pp. 35–46. DOI: 10.7892/boris.80303.
- Davis, J., T. Herring, I. Shapiro, A. Rogers, and G. Elgered (1985). Geodesy by radio interferometry: Effects of atmospheric modeling errors on estimates of baseline length. *Radio science*, **20**(6), 1593–1607. DOI: 10.1029/RS020i006p01593.
- Diamantidis, P.-K., G. Klopotek, and R. Haas (2020). VLBI and GPS inter- and intra-technique combinations on the observation level for evaluation of TRF and EOP. *Earth, Planets and Space*. in review.
- Ejigu, Y. G., A. Hunegnaw, K. E. Abraha, and F. N. Teferle (2019). Impact of GPS antenna phase center models on zenith wet delay and tropospheric gradients. *GPS Solutions*, **23**(1), 5. DOI: 10.1007/s10291-018-0796-9.
- Gambis, D., J.-Y. Richard, M. Seitz, and R. Biancale (2012). Combination of Space Geodetic Techniques at the Observation Level. *cosp*, **39**, 580.
- Geng, J., X. Meng, A. H. Dodson, and F. N. Teferle (2010). Integer ambiguity resolution in precise point positioning: method comparison. *Journal of Geodesy*, **84**(9), 569–581. DOI: 10.1007/s00190-010-0399-x.
- Gipson, J. (2010). “An introduction to Sked”. *IVS 2010 General Meeting Proceedings “VLBI2010: From Vision to Reality”*. Ed. by D. Behred and K. D. Baver. NASA/CP-2010-215864, pp. 77–84.
- Griffiths, J. and J. R. Ray (2013). Sub-daily alias and draconitic errors in the IGS orbits. *GPS solutions*, **17**(3), 413–422.
- Hearn, E., S. McClusky, S. Ergintav, and R. Reilinger (2009). Izmit earthquake post-seismic deformation and dynamics of the North Anatolian Fault Zone. *Journal of Geophysical Research: Solid Earth*, **114**(B8). DOI: 10.1029/2008JB006021.
- Hernández-Pajares, M., J. Juan, J. Sanz, R. Orus, A. Garcia-Rigo, J. Feltens, A. Komjathy, S. Schaer, and A. Krankowski (2009). The IGS VTEC maps: a reliable source of ionospheric information since 1998. *Journal of Geodesy*, **83**(3-4), 263–275. DOI: 10.1007/s00190-008-0266-1.
- Hobiger, T., T. Gotoh, T. Kubooka, M. Sekido, H. Takiguchi, and H. Takeuchi (2010). “c5++-multi-technique Analysis Software for Next Generation Geodetic Instruments”. *IVS 2010 General Meeting Proceedings “VLBI2010: From Vision*

- to Reality*". Ed. by D. Behred and K. D. Baver. NASA/CP-2010-215864, pp. 212–216.
- Hobiger, T. and T. Otsubo (2015). "Combination of space geodetic techniques on the observation level with c5++: common nuisance parameters and data weighting". *REFAG 2014. International Association of Geodesy Symposia*. Ed. by T. van Dam. Vol. 146. Springer, pp. 31–37. ISBN: 978-3-319-45628-7. DOI: 10.1007/1345_2015_152.
- Hobiger, T., C. Rieck, R. Haas, and Y. Koyama (2015). Combining GPS and VLBI for inter-continental frequency transfer. *Metrologia*, **52**(2), 251. DOI: 10.1088/0026-1394/52/2/251.
- Jin, S., E. Cardellach, and F. Xie (2014). *GNSS Remote Sensing*. Springer. ISBN: 978-94-007-7481-0. DOI: 10.1007/978-94-007-7482-7.
- Johnston, G., A. Riddell, and G. Hausler (2017). "The International GNSS Service". *Springer Handbook of Global Navigation Satellite Systems*. Ed. by P. J. Teunissen and O. Montenbruck. Springer Handbooks. Springer, pp. 967–982. ISBN: 978-3-319-42926-7. DOI: 10.1007/978-3-319-42928-1_33.
- Klopotek, G., T. Hobiger, R. Haas, and T. Otsubo (2020). Geodetic VLBI for precise orbit determination of Earth satellites: a simulation study. *Journal of Geodesy*, **94**(6), 1–26.
- Kondo, T. and K. Takefuji (2016). An algorithm of wideband bandwidth synthesis for geodetic VLBI. *Radio Science*, **51**(10), 1686–1702. DOI: 10.1002/2016RS006070.
- Kotsakis, C. (Oct. 2018). "Datum Definition and Minimal Constraints". *Encyclopedia of Geodesy. Encyclopedia of Earth Sciences Series*. Ed. by E. Grafarend. Springer. ISBN: 978-3-030-15259-8. DOI: 10.1007/978-3-319-02370-0_157-1.
- Kouba, J. (2009). *A guide to using International GNSS Service (IGS) products*. <http://acc.igs.org/UsingIGSPProductsVer21.pdf>.
- Krügel, M., D. Thaller, V. Tesmer, M. Rothacher, D. Angermann, and R. Schmid (2007). Tropospheric parameters: combination studies based on homogeneous VLBI and GPS data. *Journal of Geodesy*, **81**(6-8), 515–527. DOI: 10.1007/s00190-006-0127-8.
- Kumar, S. and K. B. Moore (2002). The Evolution of Global Positioning System (GPS) Technology. *Journal of Science Education and Technology*, **11**(1), 59–80. DOI: 10.1023/A:1013999415003.
- Landskron, D. and J. Böhm (2018). VMF3/GPT3: refined discrete and empirical troposphere mapping functions. *Journal of Geodesy*, **92**(4), 349–360. DOI: 10.1007/s00190-017-1066-2.
- Laurichesse, D., F. Mercier, J.-P. Berthias, P. Broca, and L. Cerri (2009). Integer Ambiguity Resolution on Undifferenced GPS Phase Measurements and its

- Application to PPP and Satellite Precise Orbit Determination. *Navigation*, **56**(2), 135–149. DOI: 10.1002/j.2161-4296.2009.tb01750.x.
- MacMillan, D., D. Behrend, and S. Kurihara (2012). “Effects of the 2011 Tohoku earthquake on VLBI geodetic measurements”. *Proceedings 7th International VLBI Service for geodesy and astrometry 2012 General Meeting*, pp. 440–444.
- MacMillan, D., A. Fey, J. Gipson, D. Gordon, C. Jacobs, H. Krásná, S. Lambert, Z. Malkin, O. Titov, G. Wang, et al. (2019). Galactocentric acceleration in VLBI analysis-Findings of IVS WG8. *Astronomy & Astrophysics*, **630**, A93.
- Malkin, Z. (2009). On comparison of the Earth orientation parameters obtained from different VLBI networks and observing programs. *Journal of Geodesy*, **83**(6), 547–556. DOI: 10.1007/s00190-011-0483-x.
- Miller, S. and C. Wunsch (1973). The pole tide. *Nature Physical Science*, **246**(155), 98–102. DOI: 10.1038/physci246098a0.
- Montenbruck, O., P. Steigenberger, L. Prange, Z. Deng, Q. Zhao, F. Perosanz, I. Romero, C. Noll, A. Stürze, G. Weber, R. Schmid, K. MacLeod, and S. Schaer (2017). The Multi-GNSS Experiment (MGEX) of the International GNSS Service (IGS) – Achievements, prospects and challenges. *Advances in Space Research*, **59**(7), 1671–1697. DOI: 10.1016/j.asr.2017.01.011.
- Noll, C. E. (2010). The crustal dynamics data information system: A resource to support scientific analysis using space geodesy. *Advances in Space Research*, **45**(12), 1421–1440. DOI: 10.1016/j.asr.2010.01.018.
- Nothnagel, A., T. Artz, D. Behrend, and Z. Malkin (2017). International VLBI service for geodesy and astrometry. *Journal of Geodesy*, **91**(7), 711–721.
- Nothnagel, A., C. Holst, and R. Haas (2019). A VLBI delay model for gravitational deformations of the Onsala 20 m radio telescope and the impact on its global coordinates. *Journal of Geodesy*, **93**(10). DOI: 10.1007/s00190-019-01299-x.
- Nothnagel, A. (2009). Conventions on thermal expansion modelling of radio telescopes for geodetic and astrometric VLBI. *Journal of Geodesy*, **83**(8), 787–792. DOI: 10.1007/s00190-008-0284-z.
- Petit, G., F. Arias, and G. Panfilo (2015). International atomic time: Status and future challenges. *Comptes Rendus Physique*, **16**(5), 480–488.
- Petit, G. and B. Luzum (2010). *IERS Conventions (2010) (IERS Technical Note)*. Vol. 36. Frankfurt am Main: Verlag des Bundesamts für Kartographie und Geodäsie, pp. 1–179. ISBN: 3-89888-989-6.
- Prange, L., E. Orliac, R. Dach, D. Arnold, G. Beutler, S. Schaer, and A. Jäggi (2017). CODE’s five-system orbit and clock solution—the challenges of multi-GNSS data analysis. *Journal of Geodesy*, **91**(4), 345–360. DOI: 10.1007/s00190-016-0968-8.

- Preston, R. A., D. Morabito, A. Wehrle, D. Jauncey, M. Batty, R. Haynes, A. Wright, and G. Nicolson (1983). VLBI observations of a radio flare of Circinus X-1. *The Astrophysical Journal*, **268**, L23–L26. DOI: 10.1086/184022.
- Ray, J. and Z. Altamimi (2005). Evaluation of co-location ties relating the VLBI and GPS reference frames. *Journal of Geodesy*, **79**(4-5), 189–195. DOI: 10.1007/s00190-005-0456-z.
- Rothacher, M., G. Beutler, T. A. Herring, and R. Weber (1999). Estimation of nutation using the Global Positioning System. *Journal of Geophysical Research: Solid Earth*, **104**(B3), 4835–4859. DOI: 10.1029/1998JB900078.
- Schartner, M. and J. Böhm (2019). VieSched++: a New VLBI Scheduling Software for Geodesy and Astrometry. *Publications of the Astronomical Society of the Pacific*, **131**(1002), 084501. DOI: 10.1088/1538-3873/ab1820.
- Scherneck, H.-G. and F. H. Webb (1999). “Ocean tide loading and diurnal tidal motion of the solid Earth centre”. *IERS Analysis Campaign to Investigate Motions of the Geocenter (IERS Technical Note 25)*. Ed. by J. Ray. Central Bureau of IERS - Observatoire de Paris, pp. 85–91.
- Shaffer, D. B. (2000). “RFI: Effects on Bandwidth Synthesis”. *International VLBI Service for Geodesy and Astrometry 2000 General Meeting Proceedings*. Ed. by N. Vandenberg and K. D. Bayer. NASA/CP-2000-209893, pp. 402–406.
- Sillard, P. and C. Boucher (2001). A review of algebraic constraints in terrestrial reference frame datum definition. *Journal of Geodesy*, **75**(2-3), 63–73.
- Sovers, O. J., J. L. Fanselow, and C. S. Jacobs (1998). Astrometry and geodesy with radio interferometry: experiments, models, results. *Reviews of Modern Physics*, **70**(4), 1393. DOI: 10.1103/RevModPhys.70.1393.
- Springer, T., F. Dilssner, D. Escobar, C. Flohrer, O. Otten, D. Svehla, and R. Zandbergen (2011). NAPEOS: The ESA/ESOC tool for Space Geodesy. *Geophysical Research Abstracts*, **13**. EGU2011-8287.
- Teunissen, P., P. Joosten, and C. Tiberius (2002). “A comparison of TCAR, CIR and LAMBDA GNSS ambiguity resolution”. *Proceedings of the 15th International Technical Meeting of the Satellite Division of the Institute of Navigation (ION GPS 2002)*, pp. 2799–2808.
- Thaller, D. (2008). “Inter-technique combination based on homogeneous normal equation systems including station coordinates, Earth orientation and troposphere parameters”. PhD thesis. Technische Universität München.
- Thaller, D., R. Dach, M. Seitz, G. Beutler, M. Mareyen, and B. Richter (2011). Combination of GNSS and SLR observations using satellite co-locations. *Journal of Geodesy*, **85**(5), 257–272. DOI: 10.1007/s00190-010-0433-z.
- Walpersdorf, A., E. Calais, J. Haase, L. Eymard, M. Desbois, and H. Vedel (2001). Atmospheric gradients estimated by GPS compared to a high resolution nu-

- merical weather prediction (NWP) model. *Physics and Chemistry of the Earth, Part A: Solid Earth and Geodesy*, **26**(3), 147–152. DOI: 10.1016/S1464-1895(01)00038-2.
- Whitney, A., A. Rogers, H. Hinteregger, C. Knight, J. Levine, S. Lippincott, T. Clark, I. Shapiro, and D. Robertson (1976). A very-long-baseline interferometer system for geodetic applications. *Radio Science*, **11**(5), 421–432. DOI: 10.1029/RS011i005p00421.
- Williams, S. and N. Penna (2011). Non-tidal ocean loading effects on geodetic GPS heights. *Geophysical Research Letters*, **38**(9). DOI: 10.1029/2011GL046940.
- Wresnik, J., R. Haas, J. Boehm, and H. Schuh (2007). Modeling thermal deformation of VLBI antennas with a new temperature model. *Journal of Geodesy*, **81**(6-8), 423–431. DOI: 10.1007/s00190-006-0120-2.

Paper I

VLBI and GPS inter- and intra-technique combinations on the observation level for evaluation of TRF and EOP

P.-K. Diamantidis et al. (2020). VLBI and GPS inter- and intra-technique combinations on the observation level for evaluation of TRF and EOP. *Earth, Planets and Space*. in review

1 **VLBI and GPS inter- and intra-technique combinations on the**
2 **observation level for evaluation of TRF and EOP**

3 Periklis-Konstantinos Diamantidis, Department of Space, Earth and Environment, Chalmers
University of Technology, Gothenburg, Sweden, periklis.diamantidis@chalmers.se

Grzegorz Kłopotek, Department of Space, Earth and Environment, Chalmers University
of Technology, Gothenburg, Sweden, grzegorz.kłopotek@chalmers.se, (now at ETH Zürich,
kłopotek@ethz.ch)

Rüdiger Haas, Department of Space, Earth and Environment, Chalmers University of
Technology, Gothenburg, Sweden, rudiger.haas@chalmers.se

5 **Abstract**

6 We study the effects of combination on the observation level of different space-geodetic techniques and
7 of networks of the same technique and present the corresponding improvement for the determination of
8 station positions and earth orientation parameters. Data from the continuous geodetic very long
9 baseline interferometry (VLBI) campaign CONT17 are used in a batch least-squares estimator. This
10 campaign includes 15 days of observations with two legacy S/X networks, namely Legacy-1 (L1) and
11 Legacy-2 (L2). For this study the VLBI L1 network is used as the base and reference solution. Data
12 from the L1 network are combined first with data from co-located Global Positioning System (GPS)
13 stations by estimating common tropospheric parameters. The derived station positions repeatabilities
14 of the VLBI and GPS networks are evaluated with respect to single-technique solutions. We find a 25 %
15 improvement in terms of precision as compared to the corresponding GPS-only and VLBI-only
16 solutions. Furthermore, a combined solution using data of the L1 and L2 network is performed by
17 estimating common earth orientation parameters. The combined L1&GPS and L1&L2 solutions are
18 compared to the reference solution by investigating UT1 and polar motion estimates. UT1 is evaluated
19 in terms of mean bias and formal errors with respect to the International Earth Rotation Service
20 (IERS) C04 products which were used as a priori values. We find that out of the three examined
21 solutions, the combined L1&GPS solution has the lowest formal error and mean bias for UT1 with a
22 30 % improvement. The weighted root mean square (WRMS) differences between the obtained polar
23 motion estimates and the ones derived by the International GNSS Service (IGS) are also compared. We
24 find that the combined L1&L2 solution gives the lowest WRMS, a 20 % improvement with respect to
25 the reference solution. The presented results highlight the potential of combinations on the observation
26 level for ongoing transition to multi-space geodetic analysis, e.g. Global Navigation Satellite Systems
27 (GNSS) with the fully operational Galileo and Beidou, and to the next generation VLBI system.

28 **Keywords**

29 VLBI, GPS, CONT17, c5++, Combination on the observation level, TRF, EOP

30 **Introduction**

31 Two-week continuous geodetic VLBI campaigns have been organized by the International VLBI Service
32 for Geodesy and Astrometry (IVS, Nothnagel et al. 2017) every third year since 2002. These continuous
33 (CONT) VLBI campaigns provide a great opportunity to not only investigate the current performance
34 of the VLBI systems (Nilsson et al. 2014), Earth rotation (Artz et al. 2010), as well as ionosphere and
35 troposphere effects (Teke et al. 2011), but also test the feasibility of combining geodetic VLBI with
36 other space-geodetic techniques such as GNSS or SLR (Thaller et al. 2007). The objective of such a
37 combination is to provide a robust estimation and physically consistent treatment of common parameters
38 of interest such as Earth orientation parameters (EOP) or zenith wet delays (ZWD), in order to ensure
39 the highest quality and homogeneity of the final products (Rothacher et al. 2011). In addition, space-
40 geodetic techniques have different strengths and weaknesses for recovering global geodetic parameters.
41 Their combination is thus beneficial to fully exploit the strengths of each of them and overcome the
42 technique-specific weaknesses (Artz et al. 2012), assuming that the combination is properly constructed,
43 suitable weights are applied and good quality ties at co-location sites are available. One such example
44 could be the scale parameter and geocenter coordinates that can be transferred from SLR to the GNSS
45 network, in the case of a combined SLR-GNSS solution (Sośnica et al. 2019). The inclusion of geodetic
46 VLBI into the solution on the other hand provides the full EOP information (Sovers et al. 1998), which
47 can augment the GNSS or SLR data analysis. Utilization of many space-geodetic techniques also improves
48 the global geometrical coverage, the quantity of observations and their density, and helps in the reduction
49 of correlations between the estimated parameters.

50 The combination of observed data originating from different space-geodetic techniques is usually carried
51 out using three different strategies in order to estimate common parameters of interest:

52 (1) CRL (combination on the result level) refers to a case where target parameters are estimated firstly
53 from single-technique solutions and the results are combined in the subsequent stage to obtain one
54 set of estimates (Seitz 2015).

55 (2) CNL (combination on the normal equation level) implies that parameters of interest such as EOP,
56 station coordinates or common troposphere models are estimated using technique-specific datum-free
57 normal equation (NEQ) systems while including necessary local tie information (Thaller et al. 2007;
58 Rothacher et al. 2011).

59 (3) COL (combination on the observation level) implies that common inter-technique as well as

60 technique-specific parameters are estimated simultaneously, preserving all correlations between the
61 estimated parameters (Coulot et al. 2007).

62 COL has already been performed (Hobiger and Otsubo 2014; Hobiger et al. 2014), but still has not been
63 yet fully exploited (Coulot et al. 2007).

64 The advent of the next-generation VLBI system, known as VGOS (VLBI Global Observing System), as
65 well as the full deployment of few Global Navigation Satellite Systems (GNSS) like Galileo and BeiDou
66 gives rise to the exciting new prospects which come from (a) the densification of observations and (b) the
67 densification of networks. In this study, we employ COL and use the CONT17 data set to examine those
68 two densification modes with respect to primary parameters of interest, namely the terrestrial reference
69 frame (TRF) and EOP. Regarding the densification of observations, data from GPS stations which are
70 co-located to the VLBI stations are used. As a consequence, the significantly improved spatio-temporal
71 observation resolution allows to derive troposphere-related parameters with improved quality, affecting
72 positively also the derived station positions and EOP. Regarding the densification of networks, the two
73 S/X VLBI networks that participated in CONT17 are combined via the common access to EOP. The
74 resulting extended network with superior global geometrical coverage improves the sensitivity to EOP
75 determination.

76 We provide the description of the input data used in this study in the *Input Data* section. The *Methods*
77 section discusses various aspects of the combination of VLBI and GPS as well as multiple VLBI networks
78 on the observation level. The *Results* section presents the obtained results, where parameters of interest
79 are derived from single- and multi-technique solutions. In the *Discussion* section we discuss the challenges
80 related to the combination of both space-geodetic techniques and comment on the discrepancies between
81 the parameters of interest derived from single-technique solutions. Finally, the *Conclusions* section
82 provides the reader with the summary and conclusions, and outlines future work concerning this topic.

83 **Input data**

84 The VLBI data set used in this study covers 15 days of CONT17 from a fourteen-station S/X network,
85 referred to as the Legacy-1 (L1) network and a thirteen-station S/X network referred to as the Legacy-2
86 (L2) network (Behrend et al. 2017). We focus on the first network as the reference for this study since all
87 involved sites have both geodetic VLBI and GPS instrumentation, which is not the case for the second
88 one. For this reason, the L2 network serves only as a complementary network to achieve improved global

89 coverage and its contribution is measured via the effect on EOP estimation. Thus, station positions for
 90 the L2 network are neither presented nor evaluated. The considered time period spans from November 28
 91 at 00:00 UTC to December 12 at 23:59 UTC. We use the data from the co-located GPS stations, which
 92 are part of the International GNSS Service (IGS). Table 1 shows the participating sites of the Legacy-1
 93 network and their VLBI and GPS stations, while Figure 1 depicts their geographical distribution.

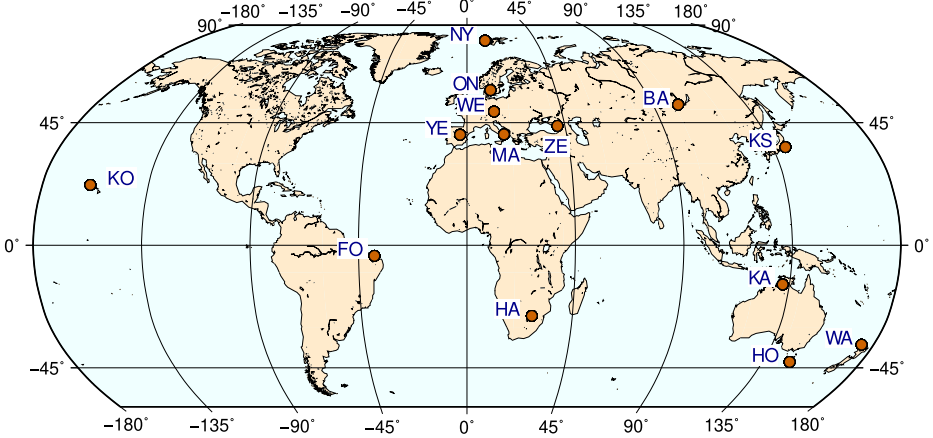


Figure 1. VLBI stations participating in the CONT17 Legacy-1 network.

94 The geodetic VLBI data are stored in the vgosDb format (Gipson 2014), where each 24-hour set of
 95 observations corresponds to a single vgosDb database. We used the analysis-ready version of the
 96 databases, commonly known as version-4 databases, where the group delay ambiguities are already
 97 resolved, ionosphere delays estimated and prospective clock breaks detected. The geodetic VLBI analysis
 98 was carried out using the S/X source catalogue of the 3rd realization of the International Celestial
 99 Reference Frame (ICRF3) (Charlot et al. 2020). In order to analyze the GPS observations in the static
 100 Precise-Point Positioning (PPP) mode, we used observation data in the Receiver INdependent EXchange
 101 (RINEX) format from the same period and IGS final products comprising satellite ephemerides and both
 102 satellite and IGS station clocks (International GNSS Service 2020).

103 **Methods**

104 Combination of space-geodetic techniques promises to provide a consistent set of nuisance parameters such
 105 as station clocks, ZWD and related tropospheric gradients in north (GRN) and east (GRE) directions.

Table 1. Geodetic core sites of the Legacy-1 network used in this study. Given are the site name, a 2-character identification (ID), and names of the co-located VLBI and GPS stations.

Site name	ID	VLBI station	GPS station
Badary	BA	BADARY	BADG
Fortaleza	FO	FORTLEZA	BRFT
Hartrao	HA	HART15M	HRAO
Hobart	HO	HOBART26	HOBA
Kashima	KS	KASHIM11	KSMV
Katherine	KA	KATH12M	KAT1
Kokee	KO	KOKEE	KOKB
Matera	MA	MATERA	MATE
Ny-Ålesund	NY	NYALES20	NYA1
Onsala	ON	ONSALA60	ONSA
Warkworth	WA	WARK12M	WARK
Wetzell	WE	WETTZELL	WTZZ
Yebe	YE	YEBES40M	YEBE
Zelenchukskaya	ZE	ZELENCHK	ZECK

106 The inclusion of local tie information and inter-technique weighting allow to identify the presence of
107 technique-specific errors and deficiencies in the modelling as well as outliers and artifacts that might be
108 present in the data. As outlined before, the combination on the observation level (COL) is the most
109 promising approach for this purpose. However, before the combination takes place, it is necessary to first
110 assess the single-technique solutions and study the behaviour and quality of the common parameters of
111 interest.

112 **Common troposphere parameters** With the co-located GPS and VLBI stations it is possible to
113 use one troposphere model that can be applied to both techniques, provided that there is a small spatial
114 distance between the co-located GPS and VLBI reference points, i.e., they share the same atmospheric
115 conditions. The common troposphere model requires consistent modelling of the hydrostatic delays. This
116 is achieved by applying the GPT3 model (Lagler et al. 2013) and using model-based pressure values that
117 are calculated for a given height of the reference points of the co-located stations. The height differences

118 also imply slightly different ZWD for the co-located stations. However, the effect was found to be rather
 119 small for the 14 sites used in the study, mainly below the standard deviation of the estimated ZWD, and
 120 thus is neglected so far in the study. The values can be calculated according to Rothacher et al. (2011)
 121 and are listed in Tab. 2 along with the RMS differences between the VLBI-derived and GPS-derived
 122 tropospheric parameters (ZWD, GRN, GRE) at the co-located stations.

Table 2. The expected ZWD differences (δ ZWD) due to the height difference between the VLBI and GPS
 reference points (Rothacher et al. 2011), shown together with the RMS differences and mean biases
 between the VLBI-derived and GPS-derived ZWD. The statistics are calculated based upon 15 daily
 single-technique solutions. Both δ ZWD and biases are expressed w.r.t. the VLBI-derived parameters.

Site	δ ZWD [mm]	ZWD [mm]	
		RMS	Bias
BA	0.25	3.5	-1.3 ± 2.0
FO	0.25	7.2	3.1 ± 4.6
HA	-0.61	7.1	-0.2 ± 3.8
HO	2.08	6.7	-3.0 ± 2.8
KS	0.38	11.7	-3.1 ± 5.2
KA	0.97	4.7	-0.3 ± 2.5
KO	0.78	8.5	-2.4 ± 4.2
MA	0.54	3.8	2.7 ± 0.7
NY	0.07	5.8	0.9 ± 4.2
ON	0.67	4.4	2.3 ± 2.1
WA	1.59	8.5	0.5 ± 3.1
WE	0.15	4.4	-0.2 ± 1.2
YE	0.99	5.5	-2.1 ± 3.1
ZE	0.40	12.2	8.1 ± 3.3

123 **Common clock parameters** In principle, it is possible to estimate a common clock correction for
 124 both considered techniques (with some inter-technique clock offsets) as usually reference signals from
 125 Hydrogen masers (H-masers) provide the same frequency standard to both GPS receivers and VLBI
 126 backends at the core sites (Hobiger and Otsubo 2014). To assess the feasibility of using a common clock

127 model for our purposes, an analysis of the clock behavior of all participating GPS receivers was carried
 128 out using the GIPSY/OASIS II software package (Webb and Zumberge 1995).
 129 The Modified Allan Standard Deviation (MDEV) calculated for three badly performing and a well
 130 performing GPS stations is shown in Fig. 2. The unusual behaviour of some of the GPS receivers includes
 131 the case of ZECK, where a loss of lock to the reference signal was detected for the GPS receiver on day
 132 7 of CONT17. In addition, clock breaks were detected for stations BADG and HRAO. Moreover, not all
 133 of the GPS receivers at the CONT17 sites were connected to the H-maser. Therefore, the combination of
 134 clocks was not pursued in this study and clocks for the co-located VLBI and GPS stations were modelled
 135 as separate parameters. Information on the VLBI and GPS clock parameterization used in this study is
 136 given in subsection *Parameter estimation*.

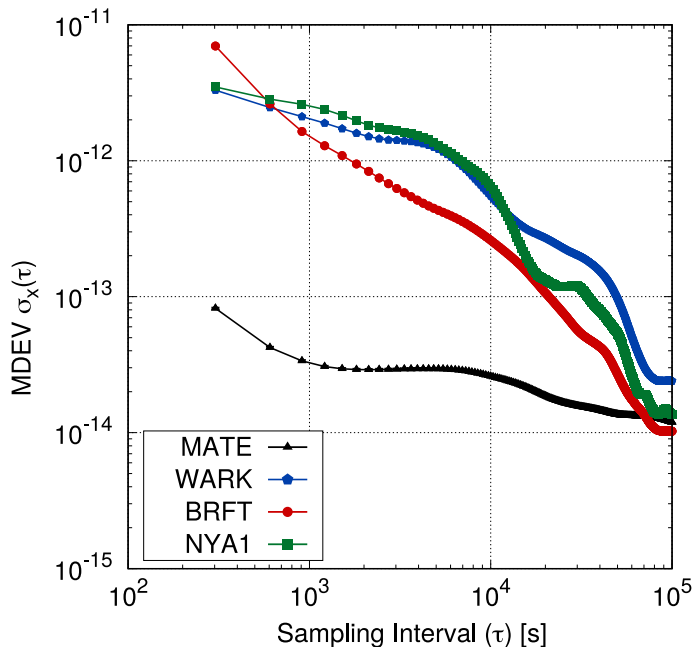


Figure 2. Frequency stability of GPS receivers on the basis of the calculated MDEV statistics for four GPS stations. The figure includes the badly performing receivers (WARK, BRFT, NYAL) and a well performing clock (MATE), which represents a general performance of other GPS receivers used in this study.

137 **Combination of different VLBI networks**

138 The L1 and L2 networks do not have co-located stations for any site, apart from the WE, and thus
139 common troposphere resolution cannot be obtained. The strength of this combination approach comes
140 from the fact that two different geometries are combined into one and hence EOP estimates of an improved
141 quality are possible. However, special consideration must be given when formulating the problem with
142 respect to how minimal constraints should be applied in order to remove the rank deficiency present in
143 that case.

144 **Application of minimal constraints** Geodetic observations usually prevent from a reliable defini-
145 tion of all components of the coordinate system (origin, orientation, and scale) with respect to which the
146 station positions are estimated. This issue, in the geodetic network adjustment, leads to a rank-deficient
147 system of NEQ. The most common approach for addressing this issue is to apply the so-called minimal
148 constraints (MC) realized in the form of No-Net-Translation (NNT), No-Net-Rotation (NNR) or No-Net-
149 Scale (NNS) conditions (Altamimi et al. 2002). The philosophy behind MC is that the number of the
150 constraints is exactly equal to the rank defect of the normal matrix.

151 The normal matrix which is constructed using observations from a single VLBI network has a rank defect
152 of 6. Thus MC are fulfilled by applying NNT and NNR, i.e., specifying the origin and orientation of the
153 realised frame to be that of the a priori frame. When combining VLBI networks and since there is no
154 direct connection with common observations between stations of different networks, there will be still two
155 distinct frame realisations with different origins, thus applying NNT constraints separately on the two
156 networks. For consistency in EOP determination, the orientation of the two frames must be common and
157 thus a single NNR constraint is applied on the combined L1&L2 network. Furthermore, MC are sensitive
158 to noisy observations and inaccurate a priori information on station coordinates, so-called data noise and
159 datum noise effect respectively. Thus a correct choice of stations to apply NNT/NNR is important for the
160 quality of the solution. In our case, the NNT/NNR constraints were imposed on twelve out of fourteen
161 VLBI stations on the L1 network and on the complete L2 network. In the case of L1, the KASHIM11
162 station was excluded from the datum constraint as it experienced severe radio frequency interference at
163 X-band, which led to the exclusion of four X-band channels at the correlation stage. The ZELENCHK
164 station was also excluded as it was found that the a priori position was suboptimal due to significant
165 discrepancy on the (fixed) station velocity information with respect to the co-located ZECK GPS station.

166 **Parameter estimation**

167 The CONT17 data were analyzed as 15 daily solutions. Four different analyses were carried out, namely an
168 VLBI L1-network only (sol-V), a GPS-only (sol-G) a combined VLBI L1&GPS (sol-VG) and a combined
169 VLBI L1&L2 (sol-VV). All available VLBI data were used (scheduled with an elevation cutoff angle
170 of 5°). The GPS data however, were decimated from the original 30-second sampling to the 5-minute
171 sampling and an elevation cut-off angle of 10° was applied to all GPS stations.

172 A two-stage parameter estimation process for all solutions was employed. First, the data were used to
173 estimate a second-order polynomial for station clocks. For L1 and L2 networks in particular, one station
174 clock per network was fixed and used as reference. Then using the polynomial as a priori information and
175 thus removing the trend from the clock parameters a second-stage estimation was performed. Station
176 clocks, zenith wet delays and tropospheric gradients were modelled as continuous piecewise linear (PWL)
177 offsets, while EOP were estimated as constant daily offsets. The time resolution of the PWL parameters
178 varied according to the temporal resolution of the dataset and are presented in detail in Tab. 3.

179 In the processing of GPS data, phase ambiguities were resolved as floats. In addition, an elevation-
180 dependent weighting was used where formal errors of each observation are multiplied with the wet mapping
181 function evaluated for a given observation elevation angle. For geodetic VLBI data, besides the formal
182 uncertainty derived at the post-correlation analysis stage, the observation error in our analysis includes
183 quantities evaluated for two stations forming a baseline, i.e., wet mapping functions computed for the
184 given elevation angles. No correlations between the individual observations were considered in our case. In
185 the case of VLBI, baseline-based variance component estimation (VCE) of the Helmert type is employed.
186 In the case of GPS, the VCE is computed per station and per type of observable (code- or carrier-
187 phase). For both GPS and VLBI, the a priori positions at each observation epoch were calculated using
188 station positions and velocities expressed in ITRF2014, including the post-seismic displacement model
189 (Altamimi et al. 2016). In terms of the periodic displacements triggered by geodynamical phenomena,
190 the modelling approach applied here followed the IERS conventions (Petit and Luzum 2010). The tidal
191 S1-S2 atmospheric loading (Ray and Ponte 2003) was also used and applied to the positions of both VLBI
192 and GPS reference points. EOP were estimated as corrections to the a priori IERS-14-C04 (Bizouard
193 et al. 2019) values.

Table 3. Parameterization of the target parameters. Presented are parameter type and temporal resolution that are used for the four different solutions. ONS and FDV stand for the VLBI station ONSALA60 and FD-VLBA, respectively. AR refers to constant offsets with non canonical timelengths as calculated by the GPS phase ambiguity resolution mode of c5++.

		sol-V	sol-G	sol-VG	sol-VV
parameter	parameter type	temporal resolution / information			
ZWD	PWL offset	1 h	0.5 h	0.5 h	1 h
Trop. gradients	PWL offset	12 h	6 h	6 h	12 h
VLBI clock reference	–	ONS	–	ONS	ONS/FDV
Station clocks	2nd order polynomial	⊗	⊗	⊗	⊗
Station clocks	& PWL offset	1 h	5 min	5 min	1 h
EOP	constant offset	24 h	–	24 h	24 h
Station coordinates	constant offset	24 h	24 h	24 h	24 h
GPS phase ambiguities	constant offset	–	AR	AR	–
Clock constraints	–	72 ps/h	36 ns/h	72 ps/h (V) 36 ns/h (G)	72 ps/h
ZWD constraints	–	32 mm/h	32 mm/h	32 mm/h	32 mm/h

194 Results

195 The effect of combination on the L1 network by employing COL of VLBI with co-located GPS stations
196 is examined in the following context. First, the derived station positions are evaluated w.r.t. the results
197 of single-technique solutions; during the performed COL the common troposphere model (ZWD, GRN,
198 GRE) was derived based on both GPS and VLBI observations. The EOP determination is then com-
199 pared w.r.t. the single-technique solution and to a solution where network densification is achieved via
200 the combination of both interferometric networks L1&L2 (sol-VV).

202 Station position repeatabilities

203 The 3D position repeatabilities are shown both (a) for the co-located L1 and GPS networks (Fig. 3)
204 and (b) for station-specific cases (Figs. 4-6). In the first case, the improvement that COL induces is

205 visible between the sol-V, sol-G and sol-VG solutions by the different color opacity. More specifically,
 206 the analysis indicates that for the L1 network t, on average, the repeatability in the up component is
 207 reduced by 25 %. In the case of the horizontal components, we note an improvement of 16 % and 6 %
 208 in the north and east components, respectively. The GPS network on the other hand experiences the
 209 biggest improvement in the north component by 40 %, followed by the up component by 10 %, while the
 210 east shows a slight degradation of 5 %.

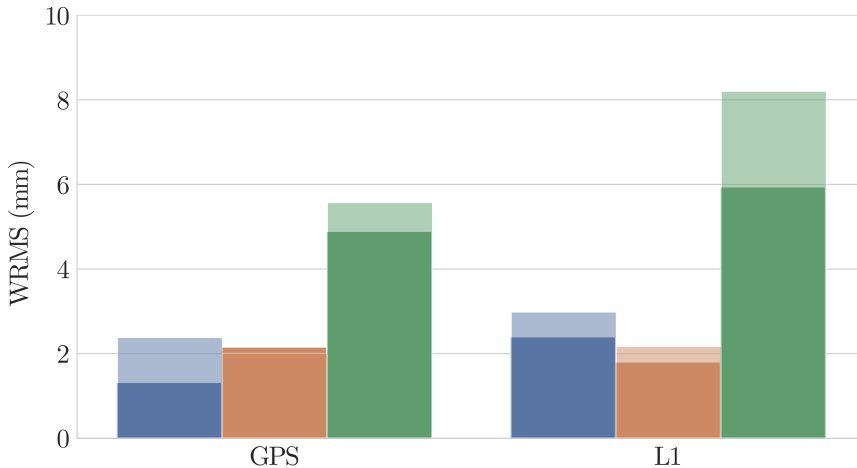


Figure 3. Station position repeatabilities (WRMS in mm) for the two co-located networks (VLBI L1 and GPS) for a) single-technique solutions, i.e. sol-V and sol-G, (faded) and b) the combined solution sol-VG (colored). The results are computed based on the 15 daily solutions. The components evaluated are north (blue), east (orange) and up (green) of the local topocentric frame.

211 Looking at station-specific results, where V stands for VLBI and G for GPS stations, direct inspection
 212 of Fig. 6 shows the relative changes. In 80 % of the cases a significant improvement is visible, varying
 213 between 10 % and 60 %. For 20 % of the cases, a small degradation is visible mainly in the GPS network
 214 with the exception of HA and YE sites, where the degradation is visible on the co-located VLBI station
 215 as well. Mostly, it does not exceed 18 %, except for the HA site where the GPS station shows a significant
 216 increase in the up component. Whether these relative changes are significant or not can be examined
 217 looking at the absolute level of the repeatabilities shown in Fig. 5. The L1 network is also examined w.r.t.
 218 the baseline length repeatabilities. The combined solution improves this metric considerably. Evaluated

219 at 6000 km, COL reduces the baseline repeatability by 35 % from 6.5 mm to 4.2 mm.

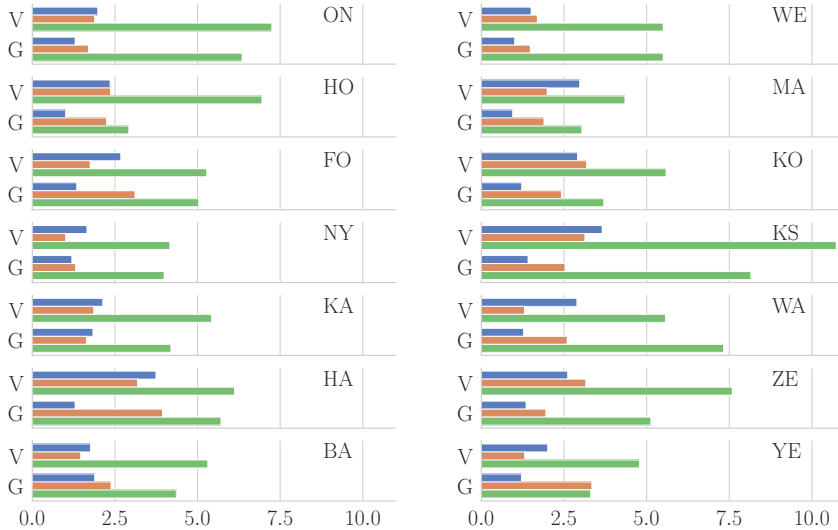


Figure 4. Station position repeatabilities (WRMS in mm) per station for the two co-located networks for sol-VG. The results are computed based upon the 15 daily solutions. The components evaluated are north (blue), east (orange) and up (green) of the local topocentric frame.

220 As shown in Tab. 4The mean RMS difference between the tropospheric parameters derived from sol-VG
 221 and sol-G is approximately 2 mm for ZWD and 0.4 mm for gradients. The average bias approaches
 222 1 mm for ZWD and 0.1 mm for the gradients. As sol-VG follows closely sol-G, it is expected that the
 223 differences of the troposphere derived from those two solutions w.r.t. sol-V will be similar. This effect
 224 is illustrated in Fig. 7, where the dominant role of sol-G to the sol-VG derived ZWD is evident, due to
 225 the characteristics of GPS observations (simultaneous observations of many satellites distributed on the
 226 local skies and a good temporal resolution of observations in relation to the VLBI technique.

227

228 EOP repeatabilities

229 EOP were evaluated augmenting the information available from the L1 network in two different ways:
 230 a) densifying the interferometric network itself by incorporating L2 network into the solution and b)
 231 better resolving the troposphere by the combined L1&GPS solution. One should keep in mind that EOP
 232 products were estimated via the L1 and/or L2 networks. The co-located GPS network was only used
 233 to better resolve troposphere and thus its effect is only indirect on the EOP estimation. While EOP

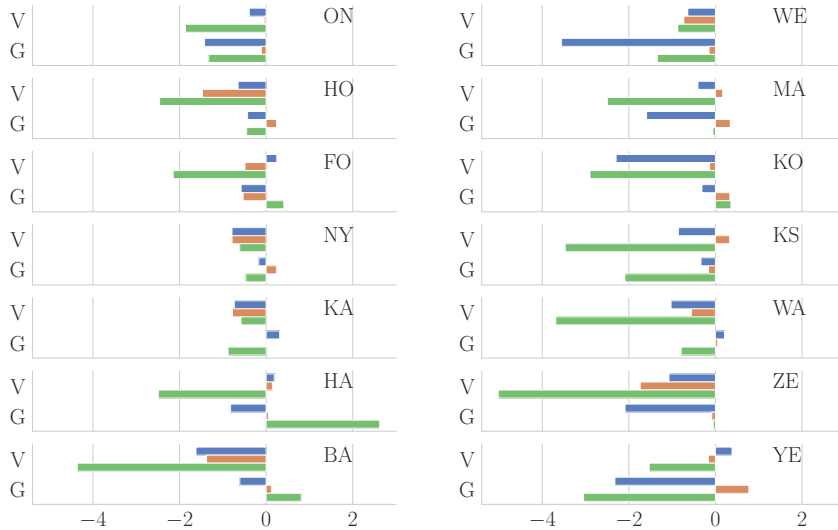


Figure 5. Absolute change in repeatabilities (WRMS in mm) per station for the two co-located networks between sol-V and sol-VG as well as sol-G and sol-VG. Negative change means that the combined solution lowers the repeatability, i.e. improvement. The components evaluated are north (blue), east (orange) and up (green) of the local topocentric frame.

234 products can be accessed through global solutions of GPS networks, those solutions routinely involve
 235 a dense network of stations, something that cannot be achieved with the geometry available from the
 236 CONT17 campaign and the combination schemes pursued in this study.

237 The process of evaluating EOP products starts with looking at UT1-UTC estimates. These estimates
 238 which were obtained from the 15 daily solutions should in principle constitute a zero-mean set. Figures 9-
 239 10 with the corresponding weighted mean offset (WMO) and formal errors show that WMO w.r.t. the
 240 a priori values are about $-19 \mu\text{as}$ for both sol-V and sol-VV, while sol-VG is causing it to drop to
 241 $-12.8 \mu\text{as}$. These results show that both combination schemes do not induce any additional bias in the
 242 solution and thus can be used to evaluate polar motion estimates. Further elaboration follows in section

243 *Discussion.*

244 Polar motion (PM) estimates (x_p, y_p) are evaluated with the aid of IGS PM products. These products
 245 have been obtained through global solutions on a dense GPS network and thus provide an excellent
 246 external reference in order to quantify the effect of the combination. The differences of the PM estimates
 247 to the IGS PM products were calculated and presented in the form of WRMS and WMO. Figures 11-12

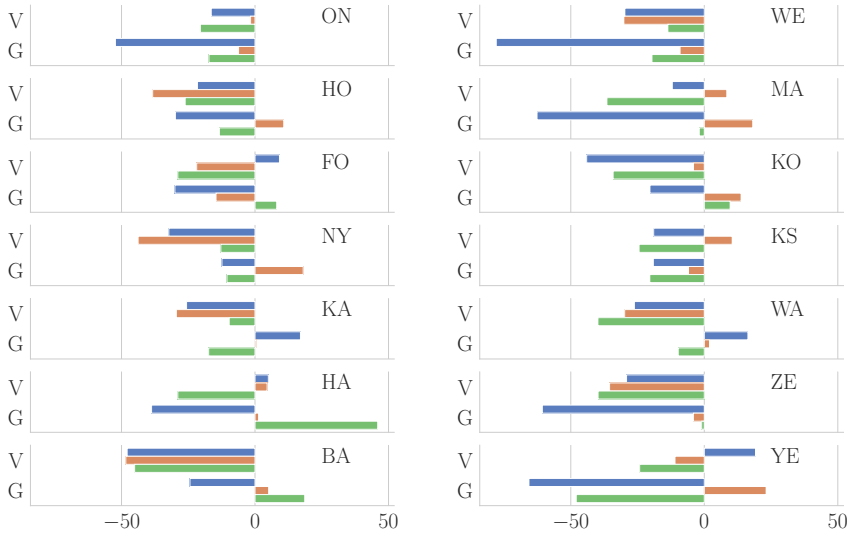


Figure 6. Relative change in repeatabilities (%) per station for the two co-located networks between between sol-V and sol-VG as well as sol-G and sol-VG. Negative repeatability changes mean that the combined solution lowers the repeatability, i.e. improvement. The components evaluated are north (blue), east (orange) and up (green) of the local topocentric frame.

248 show the effect that the combination schemes have on these two metrics. More specifically, augmentation
 249 of the L1 with the L2 network shows the biggest effect on the mean bias of x_p which lowers by 60 %,
 250 while an improvement of 10 % is also visible in the WRMS metric. The x_p component shows a 19 %
 251 improvement to the WRMS metric. COL with the co-located GPS stations also affects most the WMO
 252 of x_p which lowers by 85 %. In this case, y_p shows a bigger improvement than before, with the WMO
 253 and WRMS both decreased by 50 %. The celestial pole offsets showed non significant changes between
 254 the different combinations.

255 Discussion

256 COL was employed to augment VLBI observations performed with the use of the VLBI CONT17 Legacy-
 257 1 network (L1) in two distinctive manners. First, data from the co-located GPS stations were used and
 258 common tropospheric parameters were estimated. The aim was that GPS data with their superior
 259 temporal and spatial resolution and the simultaneous tracking of multiple satellites with a multitude
 260 of elevation and azimuth angles would allow for a better resolution of the tropospheric elongation.

Table 4. RMS differences and mean biases between the estimated ZWD derived from sol-VG and sol-V (left column) and sol-G (right column), respectively. The biases are expressed w.r.t. the sol-VG derived parameters.

Site	ZWD [mm]			
	RMS	Bias	RMS	Bias
BA	4.1	-0.4 ± 1.6	2.1	0.9 ± 0.4
FO	9.4	3.5 ± 6.0	3.6	-1.6 ± 4.5
HA	7.2	-0.8 ± 2.1	2.7	-1.5 ± 0.5
HO	7.4	-2.9 ± 3.9	2.1	0.5 ± 0.5
KS	15.4	-7.6 ± 6.7	10.9	9.5 ± 3.3
KA	6.4	-3.6 ± 1.7	1.8	0.6 ± 0.5
KO	7.9	-2.0 ± 4.0	2.2	-0.2 ± 0.3
MA	4.1	1.7 ± 1.5	1.6	0.3 ± 0.5
NY	5.2	-0.5 ± 3.8	1.9	1.0 ± 0.6
ON	4.4	2.0 ± 1.9	1.8	-0.2 ± 0.6
WA	8.2	0.3 ± 4.1	1.9	1.0 ± 0.4
WE	3.6	0.0 ± 1.7	2.1	0.1 ± 0.8
YE	6.8	-0.2 ± 5.0	2.5	1.3 ± 1.0
ZE	12.8	11.1 ± 4.2	2.6	0.8 ± 0.6

261 Correlation between this parameter and station positions would therefore result in a lower uncertainty
262 for the latter, in principle for both co-located stations. This was confirmed by the ZWD results
263 where a significant improvement of the ZWD resolution of the L1 network was observed. In general,
264 an improved ZWD estimation affects total tropospheric delay considerably and subsequently the local
265 height of a station. This effect is visible in the significant improvement that L1 network experiences
266 in the up component. All 14 participating stations show a reduction of the repeatability between 10
267 and 50 %. The components of the horizontal plane in the local topocentric frame were also evaluated.
268 Improved estimation of tropospheric gradients should allow for lower repeatabilities on the north and east
269 components. This is confirmed for most of the cases of the L1 network with the exception of FO (north),
270 HA (north and east), MA (east) and YE (north). Out of those, the degradation for HA is less than 5 %

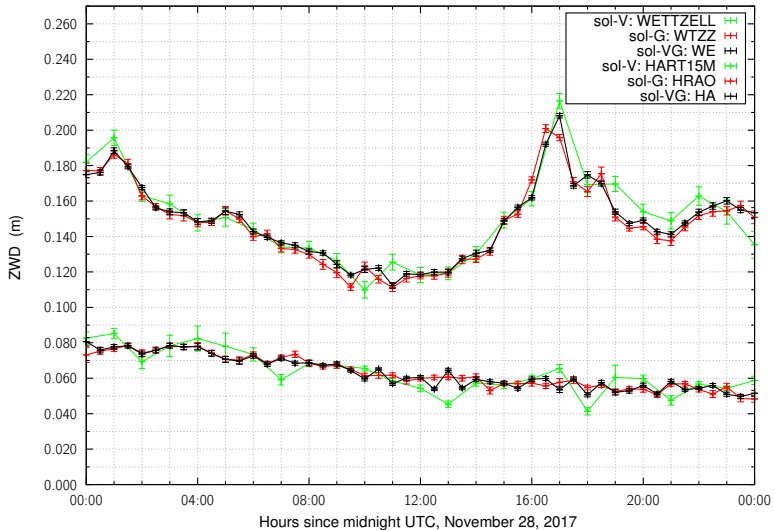


Figure 7. ZWD estimates of sol-V (green), sol-G (red), and sol-VG (black) for co-located stations at two sites, HA (top) and WE (bottom).

271 while for YE and FO the repeatability of the horizontal position components is already significantly lower
 272 than the vertical one, more than a factor of two. The east component of the MA site also follows the
 273 behavior of the horizontal position components of YE and FO and its degradation is counter-balanced
 274 by the more significant improvement in its north position component. Overall, a clear improvement can
 275 thus be observed for the L1 network station positions as an effect of the COL.

276 The results for the co-located GPS stations could also be evaluated. The improvement of the repeatabil-
 277 ities due to the presence of quasar observations may not be so visible since tropospheric estimates of the
 278 combined solution tend to be dominated by the presence of GPS. However, one can see a clear benefit on
 279 the up component in 10 out of the 14 stations where an improvement between 10 and 50 % is observed.

280 The total repeatability of the east position component for the GPS stations, co-located with the L1
 281 network, shows a slight degradation and this is visible in the station-specific evaluation as well, where a
 282 small increase in the repeatabilities is observed for 9 out of the 14 stations. The north component, on
 283 the other hand, fares better with 12 of the 14 stations showing an improvement. Taking into account
 284 that the horizontal components have comparable levels of repeatabilities, the total (net) effect on the
 285 horizontal plane is positive. Thus augmentation with quasar observations for the GPS stations allows

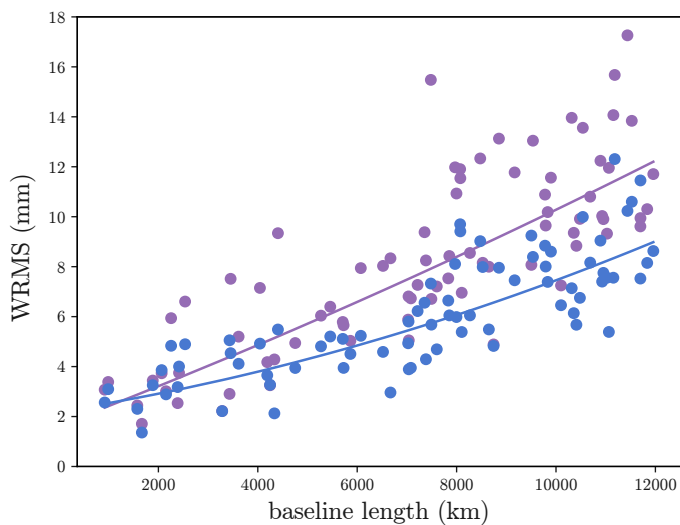


Figure 8. Baseline length repeatabilities of sol-V (blue) compared to sol-VG (magenta) for the L1 network.

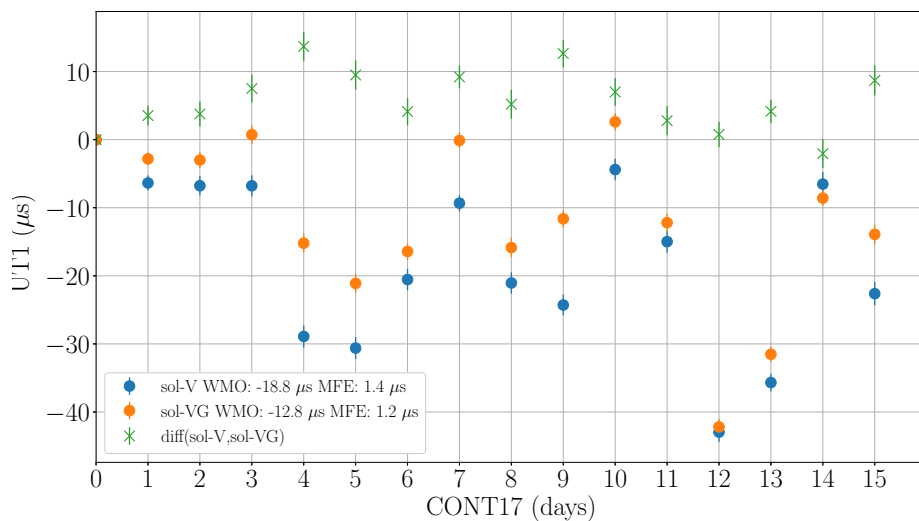


Figure 9. UT1 estimates and differences between sol-V and sol-VG. Presented are weighted mean offset (WMO) and mean formal error (MFE).

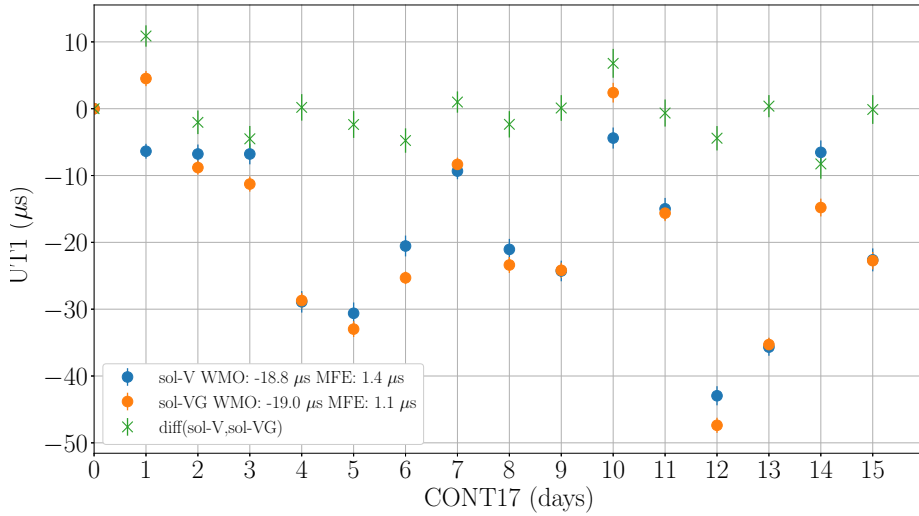


Figure 10. UT1 estimates and differences between sol-V and sol-VV. Presented are weighted mean offset (WMO) and mean formal error (MFE).

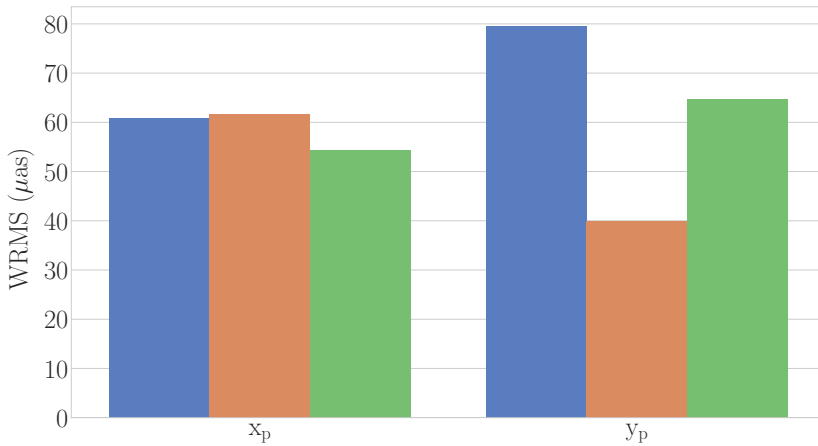


Figure 11. Polar motion (x_p , y_p) WRMS differences w.r.t. IGS PM products for sol-V (blue), sol-VG (orange), and sol-VV (green).

286 for a total improvement in the resolution of the tropospheric parameters but there might be cases where
 287 station-specific biases of the co-located VLBI station propagate into the troposphere estimates and may

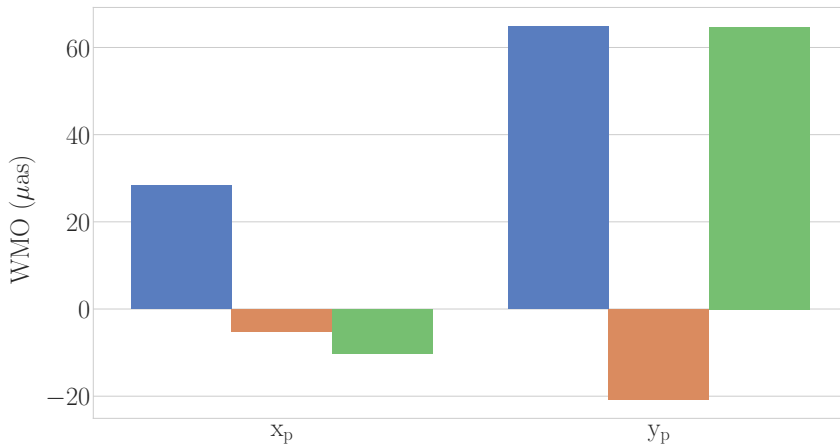


Figure 12. Polar motion (x_p, y_p) weighted mean offsets (WMO) w.r.t. IGS PM products for sol-V (blue), sol-VG (orange), and sol-VV (green).

288 cause a slight perturbation on the expected improvement of station position repeatabilities.

289 As already seen in Fig. 3, sol-V for the L1 network shows lower sensitivity on the up component with the

290 WRMS slightly above 8 mm, a factor of four more than the horizontal components. This translates to

291 baseline length repeatabilities having a monotonic quasi-linear behavior due to the major contribution of

292 the local topocentric up components on the baseline vector, as shown in Fig. 8. The effect of COL here is

293 visible in two manners, namely the total level of the WRMS and the scatter around the fitted polynom

294 (spread). The reduced total level w.r.t. the single technique solution can be deduced from what was

295 previously discussed, namely the effect of better resolved tropospheric parameters in all, but especially,

296 the up component of the station positions. The scatter shows the presence of system-specific biases,

297 like e.g., absolute (reference-formatter) time offsets, that may affect a station position estimate. More

298 specifically, a systematic error in a station position results in clusters of baselines to that station showing

299 a systematically higher WRMS than other of comparable length. For example, the VLBI station at ZE

300 is the common factor on the cluster of baselines between 2000 and 4000 km that are visibly separated

301 from the rest in sol-V. A similar situation occurs in the case of the VLBI station at KS, resulting in

302 separated clusters on the 8000 to 12000 km baseline range. For this station there were known issues

303 with the presence of radio frequency interference in 4 X-band channels and subsequent drop from the

304 correlation stage. COL is able, thus to mitigate such effects resulting in a smaller scatter around the
305 fitted polynom and visible declustering.

306 Evaluating EOP estimation and especially UT1-UTC can be challenging as there is no other technique
307 apart from VLBI which provides a direct estimate. Corrections to the C04 a priori values, obtained from
308 the 15 daily solutions should have a WMO close to zero. The existence of unmodeled system specific
309 biases like, e.g., the gravi-thermal deformation of the antennas, the sparse resolution of troposphere or
310 clock errors can propagate into UT1-UTC estimates and as is the case in this analysis where the WMO
311 is close to $-18 \mu\text{as}$. The feasibility of an attempted COL can be evaluated investigating the effect that
312 it has on the WMO of the UT1-UTC estimates. A meaningful combination scheme should result in a
313 WMO of a lower or equivalent level (Thaller 2008). Figures 9–10 show that this condition is fulfilled
314 with sol-VV resulting in a similar level and sol-VG lowering the WMO by 30 % to $-12 \mu\text{as}$.

315 PM estimates, on the other hand, have an external reference to compare to in the form IGS PM products.
316 Sol-V shows a WRMS between 60 and 80 μas which is comparable to the 40–70 μas range shown in, e.g.,
317 Nilsson et al. (2019). One would hope that both combination schemes would augment the sensitivity of
318 sol-V in both directions. Sol-VV adds more baselines in both east-west and north-south directions, while
319 sol-VG augments the information through correlation to atmospheric parameters. Inspection of the effect
320 on both WRMS and WMO, it is visible that sol-VV is more beneficial on the x_p estimation. This is due
321 to the fact that all but one stations of the L2 network are located in the northern hemisphere and hence
322 the combination adds a lot of baselines in the east-west direction, improving the sensitivity to x_p . On
323 the other hand, sol-VG shows an improvement on both x_p and y_p , where a consistent decrease of WMO
324 values on the level of 50-70 % is visible for both components as well as the WMO for x_p which is almost
325 negligible in our combination approach. As mentioned before, COL of two distinct VLBI networks, as
326 pursued here, is carried out using two networks that do not share one or multiple stations. The connection
327 between them is established by estimating common ERP and imposing the NNR constraint based on a
328 set of stations chosen from both networks. The presence of a common set of stations would additionally
329 allow for adding the NNT constraint, strengthening the combination further and allowing for enhanced
330 mitigation of network-specific biases.

331 **Conclusions**

332 The presented results indicate that the combination on the observation level is beneficial for the analysis
333 of space geodetic data. It leads to improved results for parameters of paramount interest in space geodesy,
334 i.e. TRF and EOP. Both inter- and intra-technique combinations of space geodetic observations can be
335 performed with this approach.

336 The inter-technique aspect was addressed by combining data from different techniques at co-located
337 sites, i.e. VLBI and GPS, by estimating common tropospheric parameters. VLBI and GPS data from the
338 CONT17 campaign were used for the presented approach. This combination strategy led to improvements
339 concerning determination of VLBI station positions and related baseline length repeatabilities by up to
340 25 %.

341 The intra-technique aspect was addressed by combining simultaneously observed data of the same space
342 geodetic technique, e.g. data from two different VLBI networks operating at the same time. Two VLBI
343 networks observing during the CONT17 campaign were combined by estimating a common set of EOP.
344 This combination strategy led to an improvement in precision of the derived polar motion and UT1
345 values by 20 % to 30 %, illustrated by a better agreement of our estimates with independent GPS-based
346 estimates.

347 As an outlook for the future, the plan is to extend the described COL approach within the c5++ software
348 and to combine a multitude of space geodetic techniques to address the topic in a comprehensive manner:

- 349 • Including more GPS stations than used in the presented study, not necessarily all co-located with
350 VLBI station but allowing for an adequate density and global distribution of the GPS network. This
351 may allow for determination of common EOP through direct inference from both space-geodetic
352 techniques, i.e. VLBI and GPS, with the possibility of extending the data analysis with nutation
353 components derived with the use of VLBI observations.
- 354 • Including additionally all the other existing GNSS, i.e. GLONASS, Galileo and Beidou, in the
355 combinations is a logical subsequent step and is of course expected to benefit the tropospheric
356 parameters at co-location stations, as well as the TRF and EOP determination due to an increased
357 amount of the available satellites at local skies and different orbital characteristics of those navigation
358 systems.
- 359 • Extending the COL approach by incorporating data from other techniques such as SLR, which the
360 c5++ software is already possible of analysing (Hobiger et al. 2014), is perfectly obvious and will

361 allow addressing combined EOP estimation using VLBI, GNSS and SLR.

- 362 • Additional work is required in order to extend the c5++ analysis software with other common target
363 parameters, and with the capability of utilizing DORIS and including this technique in COL.
- 364 • The final goal is to include the four major space geodetic techniques in COL within c5++ and
365 to address common troposphere (VLBI, GNSS and DORIS at co-location stations), other nuisance
366 parameters, common EOP (VLBI, GNSS, SLR and DORIS), as well as common satellite orbits
367 (GNSS and SLR for GNSS satellites that are equipped with retroreflector arrays).

368 **Availability of data and materials**

369 All used VLBI and GPS data are publically available via the international VLBI Service for Geodesy and
370 Astrometry (IVS) and the International GNSS Service (IGS), respectively.

371 **Competing interests**

372 The authors declare that there are no competing interests.

373 **Funding**

374 This work is supported by Rymdstyrelsen, the Swedish National Space Agency.

375 **Authors' contributions**

376 PKD designed the study, implemented the necessary extensions in the analysis software, analysed the
377 data, interpreted the results, prepared all graphical material, and wrote the manuscript. GK supported
378 the software extension work and result interpretation and contributed to the content of the manuscript.
379 RH supervised the work and supported the result interpretation as well as writing of the manuscript. All
380 authors read and approved the final manuscript.

381 **Authors' information**

382 PKD is a PhD student supported by Rymdstyrelsen, the Swedish National Space Agency, under project
383 number 166/16.

384 **Acknowledgements**

385 We are grateful to all parties that contributed to the success of the CONT17 campaign, in particular to
386 the IVS Coordinating Center at NASA Goddard Space Flight Center (GSFC) for taking the bulk of the
387 organizational load, to the GSFC VLBI group for preparing the legacy S/X observing schedules and MIT
388 Haystack Observatory for the VGOS observing schedules, to the IVS observing stations at Badary and
389 Zelenchukskaya (both Institute for Applied Astronomy, IAA, St. Petersburg, Russia), Fortaleza (Rádio
390 Observatório Espacial do Nordeste, ROEN; Center of Radio Astronomy and Astrophysics, Engineering
391 School, Mackenzie Presbyterian University, Sao Paulo and Brazilian Instituto Nacional de Pesquisas
392 Espaciais, INPE, Brazil), GGAO (MIT Haystack Observatory and NASA GSFC, USA), Hartebeesthoek
393 (Hartebeesthoek Radio Astronomy Observatory, National Research Foundation, South Africa), the
394 AuScope stations of Hobart, Katherine, and Yarragadee (Geoscience Australia, University of Tasmania),
395 Ishioka (Geospatial Information Authority of Japan), Kashima (National Institute of Information and
396 Communications Technology, Japan), Kokee Park (U.S. Naval Observatory and NASA GSFC, USA),
397 Matera (Agenzia Spaziale Italiana, Italy), Medicina (Istituto di Radioastronomia, Italy), Ny-Ålesund
398 (Kartverket, Norway), Onsala (Onsala Space Observatory, Chalmers University of Technology, Sweden),
399 Seshan (Shanghai Astronomical Observatory, China), Warkworth (Auckland University of Technology,
400 New Zealand), Westford (MIT Haystack Observatory), Wettzell (Bundesamt für Kartographie und
401 Geodäsie and Technische Universität München, Germany), and Yebes (Instituto Geográfico Nacional,
402 Spain) plus the Very Long Baseline Array (VLBA) stations of the Long Baseline Observatory (LBO) for
403 carrying out the observations, to the staff at the MPIfR/BKG correlator center, the VLBA correlator
404 at Socorro, and the MIT Haystack Observatory correlator for performing the correlations and the fringe
405 fitting of the data, and to the IVS Data Centers at BKG (Leipzig, Germany), Observatoire de Paris
406 (France), and NASA CDDIS (Greenbelt, MD, USA) for the central data holds.
407 IGS is acknowledged for making the GPS products available to all the interested parties.

408 **References**

409 Nothnagel, A.; Artz, T.; Behrend, D.; Malkin, Z. International VLBI Service for Geodesy and Astrometry
410 - Delivering high-quality products and embarking on observations of the next generation. *Journal of*
411 *Geodesy* **2017**, *91*, 711–721.

412 Nilsson, T.; Heinkelmann, R.; Karbon, M.; Raposo-Pulido, V.; Soja, B.; Schuh, H. Earth orientation

413 parameters estimated from VLBI during the CONT11 campaign. *Journal of Geodesy* **2014**, *88*, 491–
 414 502.

415 Artz, T.; Böckmann, S.; Nothnagel, A.; Steigenberger, P. Subdiurnal variations in the Earth’s rotation
 416 from continuous Very Long Baseline Interferometry campaigns. *Journal of Geophysical Research: Solid*
 417 *Earth* **2010**, *115*.

418 Teke, K.; Böhm, J.; Nilsson, T.; Schuh, H.; Steigenberger, P.; Dach, R.; Heinkelmann, R.; Willis, P.;
 419 Haas, R.; García-Espada, S.; Hobiger, T.; Ichikawa, R.; Shimizu, S. Multi-technique comparison of
 420 troposphere zenith delays and gradients during CONT08. *Journal of Geodesy* **2011**, *85*, 395.

421 Thaller, D.; Krügel, M.; Rothacher, M.; Tesmer, V.; Schmid, R.; Angermann, D. Combined Earth
 422 orientation parameters based on homogeneous and continuous VLBI and GPS data. *Journal of Geodesy*
 423 **2007**, *81*, 529–541.

424 Rothacher, M. et al. GGOS-D: homogeneous reprocessing and rigorous combination of space geodetic
 425 observations. *Journal of Geodesy* **2011**, *85*, 679–705.

426 Artz, T.; Bernhard, L.; Nothnagel, A.; Steigenberger, P.; Tesmer, S. Methodology for the combination of
 427 sub-daily Earth rotation from GPS and VLBI observations. *Journal of Geodesy* **2012**, *86*, 221–239.

428 Sośnica, K.; Bury, G.; Zajdel, R.; Strugarek, D.; Drożdżewski, M.; Kaźmierski, K. Estimating global
 429 geodetic parameters using SLR observations to Galileo, GLONASS, BeiDou, GPS, and QZSS. *Earth,*
 430 *Planets and Space* **2019**, *71*, 20.

431 Sovers, O. J.; Fanselow, J. L.; Jacobs, C. S. Astrometry and geodesy with radio interferometry: experi-
 432 ments, models, results. *Reviews of Modern Physics* **1998**, *70*, 1393–1454.

433 Seitz, M. Comparison of different combination strategies applied for the computation of terrestrial
 434 reference frames and geodetic parameter series. *The 1st International Workshop on the Quality of*
 435 *Geodetic Observation and Monitoring Systems (QuGOMS’11)*. 2015; pp 57–64.

436 Coulot, D.; Berio, P.; Biancale, R.; Loyer, S.; Soudarin, L.; Gontier, A.-M. Toward a direct combination
 437 of space-geodetic techniques at the measurement level: Methodology and main issues. *Journal of*
 438 *Geophysical Research: Solid Earth* **2007**, *112*.

439 Hobiger, T.; Otsubo, T. Combination of GPS and VLBI on the observation level during CONT11—
 440 common parameters, ties and inter-technique biases. *Journal of Geodesy* **2014**, *88*, 1017–1028.

441 Hobiger, T.; Otsubo, T.; Sekido, M. Observation level combination of SLR and VLBI with c5++: A case
 442 study for TIGO. *Advances in Space Research* **2014**, *53*, 119 – 129.

443 Behrend, D.; Thomas, C.; Gipson, J.; Himwich, E. Planning of the Continuous VLBI Campaign 2017
444 (CONT17). *Proceedings of the 23rd European VLBI Group for Geodesy and Astrometry Working*
445 *Meeting*. Gothenburg, 2017; pp 132–135.

446 Gipson, J. IVS Working Group IV and the New Open Format Database. *IVS 2014 General Meeting*
447 *Proceedings*. 2014; pp 248–252.

448 Charlot, P.; Jacobs, C.; Gordon, D.; Lambert, S.; de Witt, A.; Böhm, J.; Fey, A.; Heinkelmann, R.;
449 Skurikhina, E.; Titov, O., et al. The third realization of the International Celestial Reference Frame
450 by very long baseline interferometry. *Astronomy & Astrophysics* **2020**,

451 International GNSS Service, IGS products. 2020; <http://www.igs.org/products>.

452 Lagler, K.; Schindelegger, M.; Böhm, J.; Krásná, H.; Nilsson, T. GPT2: Empirical slant delay model for
453 radio space geodetic techniques. *Geophysical Research Letters* **2013**, *40*, 1069–1073.

454 Webb, F.; Zumbege, J. An Introduction to GIPSY/OASIS II, JPL D-11088. *Jet Propulsion Laboratory*,
455 *Pasadena* **1995**,

456 Altamimi, Z.; Boucher, C.; Sillard, P. New trends for the realization of the international terrestrial
457 reference system. *Advances in Space Research* **2002**, *30*, 175 – 184.

458 Altamimi, Z.; Rebischung, P.; Métivier, L.; Collilieux, X. ITRF2014: A new release of the International
459 Terrestrial Reference Frame modeling nonlinear station motions. *Journal of Geophysical Research:*
460 *Solid Earth* **2016**, *121*, 6109–6131.

461 Petit, G., Luzum, B., Eds. *IERS Conventions (2010)*; IERS Technical Note 36; Verlag des Bundesamts
462 für Kartographie und Geodäsie: Frankfurt am Main, 2010; p 179.

463 Ray, R. D.; Ponte, R. M. Barometric tides from ECMWF operational analyses. *Annales Geophysicae*
464 **2003**, *21*, 1897–1910.

465 Bizouard, C.; Lambert, S.; Gattano, C.; Becker, O.; Richard, J.-Y. The IERS EOP 14C04 solution for
466 Earth orientation parameters consistent with ITRF 2014. *Journal of Geodesy* **2019**, *93*, 621–633.

467 Thaller, D. Inter-technique combination based on homogeneous normal equation systems including station
468 coordinates, Earth orientation and troposphere parameters. Ph.D. thesis, Technische Universität
469 München, 2008.

470 Nilsson, T.; Balidakis, K.; Heinkelmann, R.; Schuh, H. Earth Orientation Parameters from the CONT17
471 Campaign. *Geophysica* **2019**, *54*, 19–25.